

$^{12}\text{C}(n,p)^{12}\text{B}$ reaction at 56, 60, and 65 MeV

F. P. Brady, T. D. Ford, G. A. Needham,* J. L. Romero, D. S. Sorenson, C. M. Castaneda,
J. L. Drummond, E. L. Hjort, B. McEachern, and N. S. P. King†
Crocker Nuclear Laboratory and Department of Physics, University of California, Davis, California 95616

D. J. Millener

Physics Department, Brookhaven National Laboratory, Upton, New York 11973

(Received 13 April 1990)

The $^{12}\text{C}(n,p)^{12}\text{B}$ reaction has been studied at 60 and 65 MeV. Cross sections for the 1^+ ground state, the 2^+ first excited state at 0.95 MeV, an unresolved pair of 2^- and 4^- states at 4.4 MeV, and the analogs of the giant electric dipole and spin-dipole resonances around 7.7 MeV have been extracted and compared with previous data at 56 MeV and with microscopic distorted-wave Born approximation calculations. The shapes of angular distributions out to $q \sim 2 \text{ fm}^{-1}$ are well reproduced by the calculations. A comparison of (n,p) , (p,n) , and (p,p') cross sections near 60 MeV is made, and a value for $|J_{\sigma\tau}|$ (the volume integral of the central, spin-isospin part of the effective nucleon-nucleon interaction) is extracted. The magnitudes of cross sections for negative-parity states can be qualitatively understood when the loose binding of the sd -shell neutron in the final state and the effect of ground-state correlations on the dipole and spin-dipole strengths are taken into account.

I. INTRODUCTION

The (n,p) reaction is important in the study of isovector transitions where one unit of isospin is transferred to the target. It is particularly selective for $N \geq Z$ targets since only analogs of $T_0 + 1$ states of the target are reached.¹ If transitions between nuclear states of definite spin and parity are involved, components of the effective nucleon-nucleon (NN) interaction can be isolated and studied. Here we present differential cross sections and analyses of the $^{12}\text{C}(n,p)^{12}\text{B}$ reaction at 60 and 65 MeV and a comparison between these sets of data and earlier (n,p) data at 56.3 MeV,² and with (p,n) and (p,p') cross sections measured near 60 MeV. The three (n,p) data sets were taken at the same neutron-beam facility, but using different detection systems,²⁻⁴ the latest being taken with the new dual-target facility which allows measurements down to 0° .

Aside from the 15.1-MeV 1^+ state, the high excitation ($T=1$) states of ^{12}C and their analogs in ^{12}B and ^{12}N have received limited study.⁵ Early (e,e') studies⁶ showed the power of back-angle electron scattering for selecting isovector magnetic transitions. Calculations⁷ verified that a large fraction of $M1$ strength was being observed in light nuclei. The nucleus ^{12}C has continued to receive considerable theoretical attention, and studies⁸⁻¹¹ indicated that, besides $M1$ strength, strong $M2$, $M3$, and $M4$ transitions should be evident to states near 19 MeV. In particular, it is predicted^{10,11} that the 19.5-MeV peak contains, in addition to $M2$, a large concentration of $M4$ strength arising from the $p_{3/2}^{-1}d_{5/2}$ particle-hole configuration. These are of particular interest because of the simplicity of this type of "stretched" configuration. A recent (e,e') experiment¹² has confirmed that the excitation strength at 19.6 MeV in ^{12}C is largely due to a $2^-, 4^-$ doublet and that additional magnetic strength ex-

ists at 20.6 and 21.7 MeV, which may be due to 3^+ and 2^- $T=1$ states, respectively. The latter paper¹² also provides a rather complete discussion of the magnetic multipole excitations in ^{12}C . The giant resonance region has also been studied via inelastic electron scattering.¹³

Early $^{12}\text{C}(n,p)^{12}\text{B}$ data² revealed the existence of prominent peaks at 0.0, 4.4, and 7.7 MeV in ^{12}B , which were identified with the excitation of a 1^+ state, a $2^-, 4^-$ doublet, and a dipole ($L=1$) resonance whose position agreed well with that of the photonuclear giant electric dipole resonance (GDR).⁵ The corresponding ^{12}C excitation energies are 15.1, 19.5, and 22.8 MeV. Data from the $^{12}\text{C}(p,n)^{12}\text{N}$ reaction¹⁴ at higher incident energies, the $^{12}\text{C}(d,^2\text{He})^{12}\text{B}$ reaction,¹⁵⁻¹⁷ radiative π^- capture,¹⁸⁻²⁰ and the $^{12}\text{C}(\gamma, \pi^+)^{12}\text{B}$ reaction,²¹ all of which excite mainly spin-isospin degrees of freedom, provide information on the distribution of spin-flip strength. The results are consistent with the interpretation that the analog 7.7-MeV structure is approximately 50% $L=1$, $S=0$ (the GDR), and 50% spin-dipole ($S=1$). Theoretically, the latter is mainly $J^\pi=1^-$, with smaller ($\approx 25\%$) contributions to the cross section from $J^\pi=0^-$ and 2^- strength. The $^{12}\text{C}(p,n)^{12}\text{N}$ reaction,^{14,22-24} the $^{12}\text{C}(^3\text{He},t)^{12}\text{N}$ reaction,^{25,26} and the $^{12}\text{C}(d,pn)^{12}\text{C}$ reaction²⁷ at a variety of incident energies, as well as the $^{12}\text{C}(n,p)^{12}\text{B}$ reaction²⁸ at 198 MeV, show spectra similar to those measured here in the $^{12}\text{C}(n,p)^{12}\text{B}$ reaction.

Section II of this paper describes the new 0° detection system and the method of data reduction used. Section III sets out the ingredients of the structure and reaction calculations. Calculated strength distributions $B(J^\pi)$ for $J^\pi=0^-, 1^-,$ and 2^- are given, and the contribution of different nuclear-structure elements to angular distributions are illustrated. Section IV presents the data for the $^{12}\text{C}(n,p)^{12}\text{B}$ reaction involving transitions to the 1^+ (ground state of ^{12}B) and the 2^+ (0.95-MeV excitation in

^{12}B), the 2^- and 4^- (4.37 and 4.52-MeV excitations in ^{12}B), and the giant dipole resonance region (6.0–9.5-MeV excitation). Comparison is made between the data and microscopic distorted-wave Born approximation (DWBA) calculations. In Sec. V the $^{12}\text{C}(n,p)^{12}\text{B}$ cross sections for the ground and first excited states are compared to the isobaric analog transitions excited in the $^{12}\text{C}(p,n)^{12}\text{N}$ and $^{12}\text{C}(p,p')^{12}\text{C}$ reactions, and a value for $|J_{\sigma\tau}|$, the volume integral of the central, spin-isospin part of the effective NN interaction, is extracted from the ground-state cross section extrapolated to $q=\omega=0$. Finally, Sec. VI contains a summary and discussion of the results obtained in this paper.

II. EXPERIMENTAL METHOD AND DATA ANALYSIS

The data presented were obtained utilizing the neutron-beam facility of the Crocker Nuclear Laboratory 76" Cyclotron.²⁹ A water-cooled ^7Li foil target is bombarded with a proton beam of approximately $12\ \mu\text{A}$ and neutrons are produced via the charge-exchange reaction $^7\text{Li}(p,n)^7\text{Be}$. The protons which do not charge exchange are swept out of the beam path by a clearing magnet into a Faraday cup. The neutrons are then collimated at 0° by a 1.55-m steel collimator giving a beam spot typically 1.8 cm wide \times 3.7 cm high and of intensity $\approx 10^6 n/s$. The neutrons travel in vacuum down the collimator and into a scattering chamber whose center is 4 m from the ^7Li production target.

A. Detection system

The detection system for the measurements at 56 MeV is described in Ref. 2. The measurements presented here at 60 MeV (Refs. 3 and 30) and at 65 MeV (Refs. 4 and 31) have in common the use of a large-area, multiwire chamber, ΔE - E , telescope system,³² but are otherwise independent of each other. The overall experimental energy resolution was 1.5 MeV for the 65-MeV data and 1.1 MeV for the 60-MeV data. The difference in resolution is due mainly to the use of a NaI detector for the 60-MeV data as opposed to a large-area plastic scintillator used in the 65-MeV setup. The setup used for the 60-MeV data allowed measurements over the angular range 7° – 33° . A bending magnet that allowed measurements down to 0° was used in the 65-MeV runs. The 65-MeV setup³³ also included a dual-target system which permitted measurements over a larger angular range (0° – 60°).

The detection system with the magnet is shown schematically in Fig. 1. The wire chambers (WC1 and WC2) allow the trajectories to be calculated, the ΔE and E detectors allow particle identification, and the $E1$ and $E2$ detectors measure the energies of the particles and provide a timing signal relative to a beam pickoff for time-of-flight selection of events due only to the full-energy neutrons from the $^7\text{Li}(p,n)^7\text{Be}$ reaction. The magnet allows detection from $\approx 15^\circ$ down to 0° from target 1, and particles originating from target 2 can be detected from $\approx 15^\circ$ to 60° . Recently, the two E detectors have been replaced by a single $15 \times 30\text{-cm}^2$ area NaI detector with $\approx 1\%$ energy resolution.

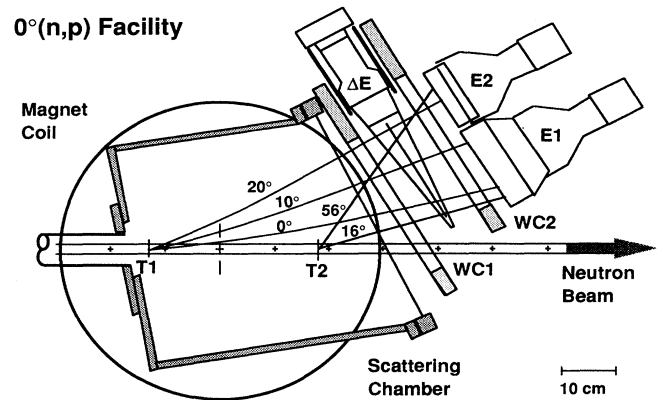


FIG. 1. Detection system showing the wire chambers (WC1 and WC2), the plastic scintillator (ΔE), NaI ($E2$), and another plastic scintillator ($E1$). Trajectories from target 1 ($T1$) are shown for 65-MeV protons scattered at 0° , 10° , and 20° . Also shown are trajectories from target 2 at 16° and 56° .

B. Data reduction

For the 60-MeV data, data reduction is relatively straightforward.^{31,32} At 65 MeV, however, the magnetic field (Fig. 1) utilized to sweep protons out of the neutron beam causes particles with different energies (momenta) to have different effective solid angles. Reference 33 describes how the spectra for each 2° or 4° angle bin are corrected so that the energy dependence in the solid angle is determined. Briefly, CH_2 targets are placed at $T1$ and $T2$ (Fig. 1), and n - p scattering events are measured for the whole energy range of the neutron beam (down to a low-energy cutoff of ~ 20 MeV). The events from $T2$ are virtually undistorted by the magnet field, and via $\sigma_{np}(\theta, E)$ one can reconstruct the neutron-beam spectrum which consists of a full-energy peak and lower-energy tail. For $T1$ events, the correction factor for each energy bin is derived from the fact that the same neutron spectrum must be derived for n - p events from CH_2 at $T1$ as from CH_2 at $T2$.

Figure 2 shows spectra from 7.5° to 31° for the 60-MeV data.³⁰ Three structures or resonances can be seen. The first resonance from the right is due to the excitation of the ground and 0.95-MeV states where the 0.95-MeV state can be unfolded from 11.5° to 31° . The second "4.4-MeV structure" is believed to be mainly due to the excitation of the 4.37-MeV (2^-) and 4.57-MeV (4^-) states, and the third resonance mainly to the 1^- giant electric ($S=0$) dipole and 0^- , 1^- , and 2^- spin-dipole states. Also shown is a phase-space continuum, assumed for the peak extraction to be due mainly to (n, np) three-body breakup. At each angle this background estimate (folded with a Gaussian to simulate the finite-energy resolution) was normalized to the data at excitation energies above the observed peaks. Figure 3 presents double-differential cross sections for the 65-MeV data which cover the angular range from 0° to 40° .³¹ In this data the 0.95-MeV state is not resolved since a plastic scintillator was used instead of the NaI detector used for the 60-MeV

data. After the continuum is subtracted, resonances are fit with Gaussian curves to help separate the peaks and obtain the net counts. A systematic uncertainty of 20% is given for states which lie above the continuum, which would include the giant dipole resonance and the 4.37 MeV + 4.52 MeV excitation. Finally, cross sections are calculated via normalization to the experimentally measured n - p cross sections.³⁴ The latter procedure produced here an overall uncertainty of $\sim 10\%$.

In the following analysis the data sets at 56.3, 60, and 65 MeV are presented with the cross sections plotted as a function of momentum transfer. When plotted this way the cross section is approximately independent of incident energy in the energy range considered, and DWBA calculations confirm this.

III. DISTORTED-WAVE AND STRUCTURE CALCULATIONS

A. Distorted-wave calculations

The distorted-wave calculations were made using the program DW81,³⁵ which includes exchange. The distorted waves were calculated using optical-model parameters based on those of Comfort and Karp.³⁶ The parameters were interpolated to the present energies, and an asymmetry potential of $24.0(N-Z)/A$ MeV was added to the potential for the outgoing $^{12}\text{B}+p$ channel. For the interaction between the incident and struck nucleons, the M3Y G -matrix³⁷ form of the effective NN interaction, as quoted by Love³⁸ (force components labeled 1, 4, 7, 8, 11,

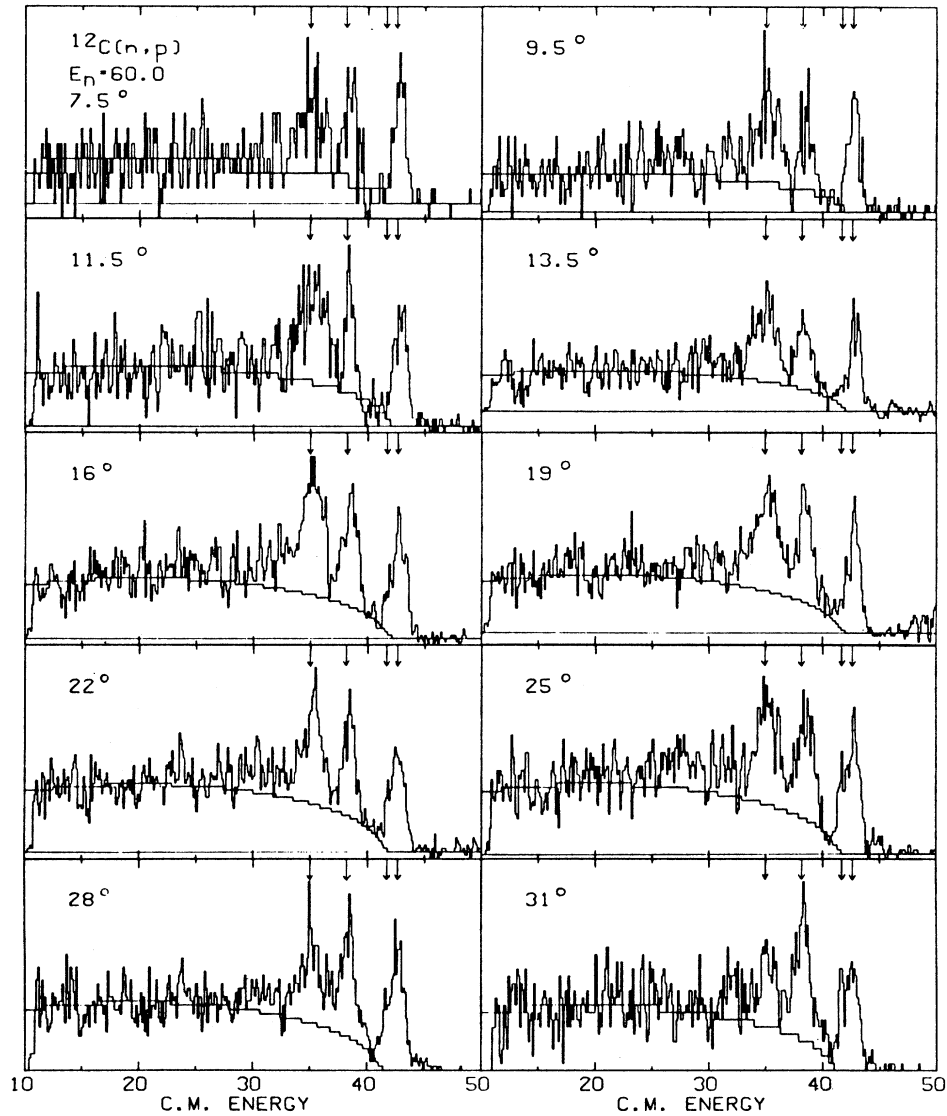


FIG. 2. Spectra for the $^{12}\text{C}(n,p)^{12}\text{B}$ reaction at 60 MeV. Four resonances are shown with the 0.95-MeV level being resolvable for angles larger than 11.5° . Also shown is the background due to three-body breakup.

14, 16, and 18 in Table 1 of Ref. 37), was used. The final ingredients required to compute a cross section are the one-body density-matrix elements (OBDM's) from a nuclear-structure calculation and single-particle wave functions for the nucleons involved in the transition.

B. Nuclear structure

The p -shell wave functions derived from the CK(POT) interaction of Cohen and Kurath³⁹ are used for the 1^+ ground state and 2^+ first excited state of ^{12}B , which contribute to the lowest peak in the $^{12}\text{C}(n,p)^{12}\text{B}$ spectrum;

the cross sections for higher positive-parity states are calculated to be small compared to those for the lowest 1^+ and 2^+ states. The isovector OBDM's for the 1^+ and 2^+ states are given in Table I in a form appropriate for input to the code DW81, which uses single-particle wave functions that are functions of the relative coordinate between the struck nucleon and core nucleus. A detailed discussion of the relationship between the standard shell-model OBDM's and those appropriate for a description in terms of relative coordinates is given elsewhere.⁴⁰ As a consequence of the coordinate transformation involved, there is a $0s_{1/2} \rightarrow 0s_{1/2}$ contribution to the 1^+ transition

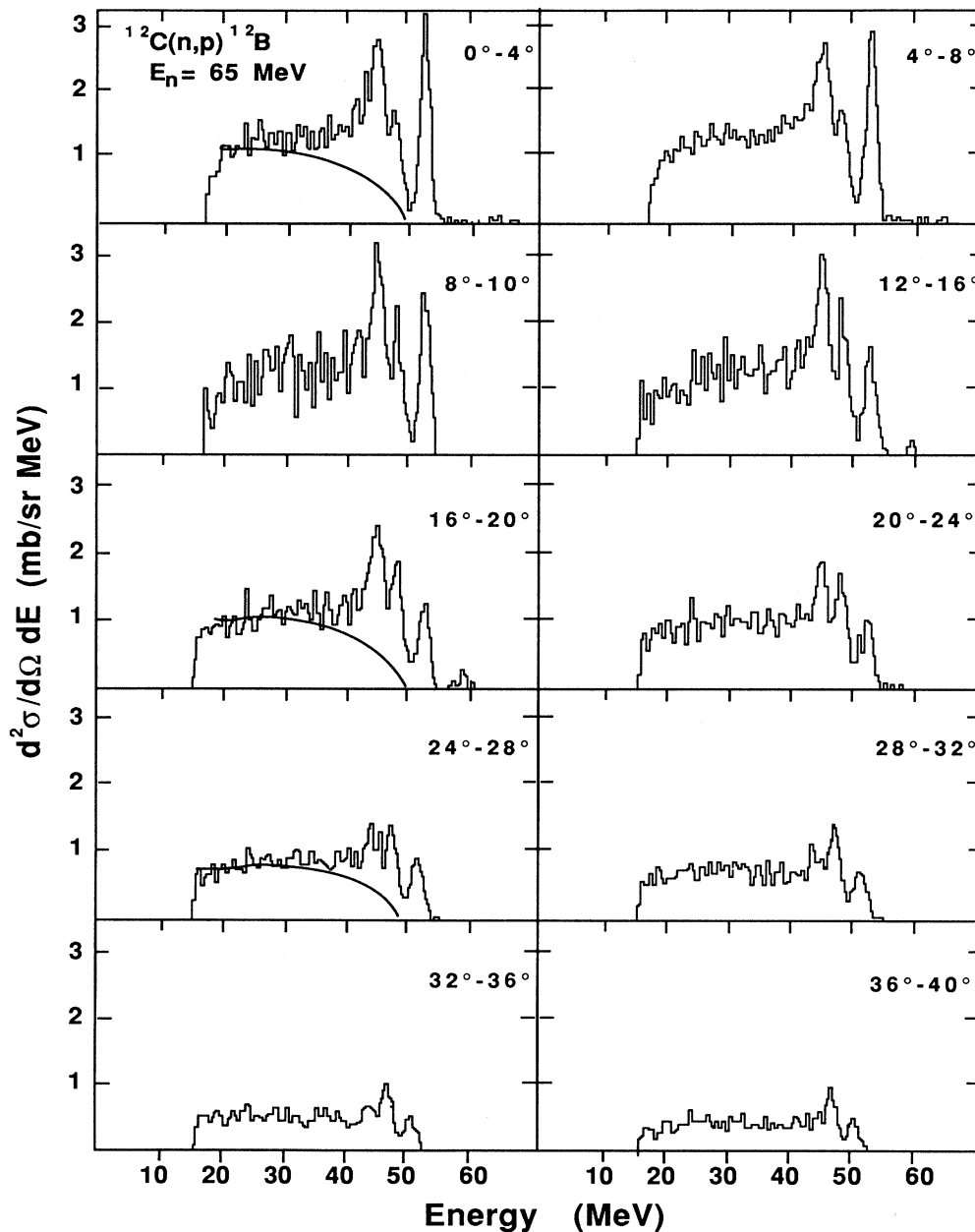


FIG. 3. Spectra for the $^{12}\text{C}(n,p)^{12}\text{B}$ reaction at 65 MeV in bins covering 4° in angle for the angular range 0° - 40° .

TABLE I. Isovector one-body density-matrix element^a for positive-parity transitions.

| J_n^π | E_x (MeV) ^b | $p_{1/2}p_{1/2}$ | $p_{1/2}p_{3/2}$ | $p_{3/2}p_{1/2}$ | $p_{3/2}p_{3/2}$ | $s_{1/2}s_{1/2}$ |
|----------------|--------------------------|------------------|------------------|------------------|------------------|------------------|
| 1 ⁺ | 0 | -0.0634 | -0.7527 | -0.3702 | -0.0834 | 0.0356 |
| 2 ⁺ | 0.95 | | 0.7418 | -0.1234 | 0.0662 | |

^aFor definitions and phase conventions, see Ref. 46.

^bTheoretical excitation energies.

density which is not present in the conventional shell-model treatment.

The shell-model calculations for the odd-parity states, which use the Millener-Kurath interaction⁴¹ in a $1\hbar\omega$ space, are described by Hicks *et al.*¹² who discuss the weak-coupling and LS structure of the low-lying $T=1$ excitations and give conventional jj -coupled OBDME's for these states. The relative coordinate OBDME's for 0^- , 1^- , and 2^- states below 10 MeV (and a 0^- state at 14 MeV) are given in Table II. The $p \rightarrow sd$ OBDME's are larger than the conventional OBDME's tabulated by Hicks *et al.*¹² by a simple factor $(\frac{12}{11})^{3/2}$, while the relationship between the $s \rightarrow p$ OBDME's in the two cases is given in the Appendix. The calculated excitation energies given in Table II differ from those given by Hicks *et al.*¹² who normalized their negative-parity spectrum to the energy of the 2^- level at 16.58 MeV in ^{12}C . Our excitation energies are, in effect, normalized to the 18.98-MeV 4^- ; $T=1$ level of ^{16}O . Then the excitation energies of states for $A=12-16$, which are strongly excited by $p \rightarrow d$ $M4$ transitions, are well reproduced. States with large $1s_{1/2}$ components, such as the 2_1^- , $T=1$ level, are predicted to be too high in energy, indicating a shortcoming of the Millener-Kurath (MK) interaction.⁴¹

From the OBDME's in the jj representation, it is difficult to see which states will be strongly populated in

inelastic-scattering reactions. Gaarde *et al.*¹⁴ have noted a rough proportionality between charge-exchange cross sections and

$$B(\Delta J; J_i T_i \rightarrow J_f T_f) = \frac{2J_f + 1}{2J_i + 1} \langle J_f T_f || (rY^1, O^{\Delta S})^{\Delta J} \tau_{\pm} || J_i T_i \rangle^2, \quad (1)$$

where we use Brink and Satchler's definition⁴² of the reduced matrix element, $O^{\Delta S}=1$ or σ for dipole or spin-dipole excitations, and $\Delta J=0, 1$, or 2 is the total angular momentum transfer. The reduced matrix element is, for harmonic-oscillator wave functions, simply proportional to the $SU(3)$ OBDME's with $(\lambda\mu)=(10)$, $\Delta L=1$, and the appropriate ΔS . In terms of LS coupling, $(\lambda\mu)=(10)$ represents $\frac{5}{6} 0p \rightarrow 0d$ and $\frac{1}{6} 0p \rightarrow 1s$ by intensity. Thus the states prominently excited in the $^{12}\text{C}(n,p)^{12}\text{B}$ reaction are dominated by $p \rightarrow d$ transitions and the energy normalization of the theoretical spectrum discussed above is most appropriate for a comparison between theory and experiment.

The distribution of strength up to 20 MeV in ^{12}B , as measured by $B^{1/2}$, is shown in Fig. 4 where a strong 2^- state at 4.5 MeV and a concentration of strength in the 6–9.5-MeV region are evident. A number of similar calculations have been performed by other au-

TABLE II. Isovector one-body density-matrix elements^a in the jj representation for negative-parity transitions.

| J_n^π | E_x (MeV) ^b | $1s_{1/2}p_{1/2}$ | $d_{3/2}p_{1/2}$ | $d_{5/2}p_{1/2}$ | $1s_{1/2}p_{3/2}$ | $d_{3/2}p_{3/2}$ | $d_{5/2}p_{3/2}$ | $p_{1/2}0s_{1/2}$ | $p_{3/2}0s_{1/2}$ |
|-----------------------------|--------------------------|-------------------|------------------|------------------|-------------------|------------------|------------------|-------------------|-------------------|
| 0 ₁ ⁻ | 4.85 | -0.6454 | | | | 0.0023 | | 0.1024 | |
| 0 ₂ ⁻ | 9.29 | 0.1146 | | | | 0.7617 | | -0.0846 | |
| 0 ₃ ⁻ | 10.16 | -0.0227 | | | | -0.0550 | | 0.3293 | |
| 0 ₄ ⁻ | 14.49 | 0.0698 | | | | -0.5134 | | -0.2378 | |
| 1 ₁ ⁻ | 3.51 | 0.1223 | 0.0036 | | -0.8172 | 0.1366 | -0.2020 | -0.0479 | 0.0384 |
| 1 ₂ ⁻ | 5.38 | -0.6016 | 0.0024 | | -0.1079 | -0.0171 | -0.0743 | -0.0341 | -0.0524 |
| 1 ₃ ⁻ | 7.56 | -0.0090 | -0.2216 | | 0.1449 | 0.3153 | -0.6519 | -0.0328 | 0.0841 |
| 1 ₄ ⁻ | 8.34 | -0.1654 | -0.2194 | | -0.1784 | 0.3618 | 0.5962 | -0.0740 | -0.1318 |
| 1 ₅ ⁻ | 9.08 | -0.0004 | 0.0226 | | -0.3643 | -0.4279 | -0.0168 | 0.0063 | -0.0148 |
| 2 ₁ ⁻ | 2.75 | | -0.0379 | 0.0054 | 0.8066 | -0.0057 | 0.3958 | | 0.0298 |
| 2 ₂ ⁻ | 4.51 | | -0.0773 | -0.3387 | -0.3661 | -0.1030 | 0.6290 | | -0.1276 |
| 2 ₃ ⁻ | 6.52 | | -0.1903 | 0.3907 | -0.1248 | -0.5471 | 0.2230 | | 0.0236 |
| 2 ₄ ⁻ | 7.27 | | -0.0523 | -0.1940 | 0.3489 | -0.4479 | -0.4280 | | 0.0677 |
| 2 ₅ ⁻ | 8.48 | | -0.2812 | -0.0751 | -0.0413 | 0.0074 | -0.1365 | | 0.0430 |
| 4 ₁ ⁻ | 4.52 | | | | | | -0.9194 | | |

^aFor definitions and phase conventions, see Ref. 46. These OBDME's are appropriate for use with single-particle wave functions which are a function of the relative coordinate between the particle and $A-1$ core. Conventional shell-model OBDME's for some of the states can be found in Table III of Ref. 12.

^bTheoretical excitation energies.

thors.^{14,25,43-45} The sum-rule strengths for $\Delta S=1$, in a calculation identical to ours, have been given by Sagawa and Brown⁴³ who find, for harmonic-oscillator wave functions with $b=1.64$ fm, $\sum B=4.56$, 12.61, and 17.48 fm² for $J^\pi=0^-$, 1^- , and 2^- , respectively. For comparison, the pure SU(3) OBDME's for $p \rightarrow sd$ excitations of the ^{16}O closed shell are unity and give

$$\sum_f B(i \rightarrow f) = \frac{3}{4\pi} (2J_f + 1) 8b^2, \quad (2)$$

independent of ΔS . Aside from different values of b , the $p \rightarrow sd$ contributions for $A=12$ are reduced by roughly a factor of $\frac{2}{3}$, reflecting the number of available p -shell nucleons, while $s \rightarrow p$ contributions increase the sum rule, mainly for $J^\pi=0^-$ and 1^- . The 1^- sum rule for $\Delta S=0$ is slightly smaller than that for $\Delta S=1$ because the $0s_{1/2} \rightarrow 1p_{1/2}$ contribution is smaller for $\Delta S=0$ than for $\Delta S=1$ (see Table VI of Ref. 46). However, it can be seen from Table II that the $s \rightarrow p$ contributions are small for the states below 10 MeV. These states exhaust a large fraction of the sum-rule strength, ranging from 55% for 0^- to 79% for 2^- . Gaarde *et al.*¹⁴ show at the top of their Fig. 5 values of $B(1^-)$ for $\Delta S=0$ transitions which are smaller, and thus in error, by a factor of ≈ 3 than the B values that we calculate. However, in Table 2 of Ref. 14, the cross sections that they calculate using the OBDME's from their shell-model calculation appear to be correct, and the contribution of electric dipole

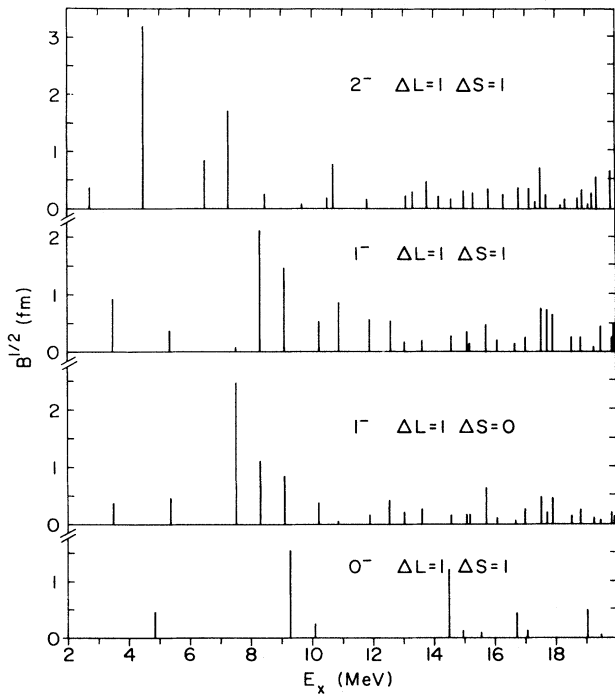


FIG. 4. Theoretical distribution of dipole and spin-dipole strength in ^{12}B . The square root of the quantity $B(\lambda; i \rightarrow f)$, defined in Eq. (1), is plotted as a function of the theoretical excitation energies of 0^- , 1^- , and 2^- states in ^{12}B .

strength to the 21.1-MeV state is in line with that expected from the ratio $(|J_{\sigma\tau}|/|J_\tau|)^2 \approx 6$ at 160 MeV.

The main purpose of Sagawa and Brown's calculation⁴³ was to estimate the reduction in sum-rule strengths from $2\hbar\omega$ 2p-2h ground-state correlations, which they found to be about 25% for the three spin-dipole modes. In the next section we show that the use of more realistic Woods-Saxon wave functions in place of harmonic-oscillator wave functions leads to an additional reduction of the DWBA cross sections by a similar factor. This happens because the p -shell proton in the initial state is rather deeply bound, while the sd -shell neutron in the final nucleus is loosely bound or unbound.

C. Single-particle wave functions

Harmonic-oscillator single-particle wave functions have commonly been used in studies of the inelastic scattering of nucleons from ^{12}C , with the oscillator parameter b chosen to obtain a reasonably good fit to the shape of electron-scattering form factors.⁴⁷ The oscillator parameters so obtained⁴⁷ can differ considerably from the value $b=1.64$ fm (the corresponding relative oscillator parameter, to be used with the OBDME's of Table I, is 1.713 fm), required to reproduce the rms charge radius of ^{12}C .

To use Woods-Saxon wave functions, we fix the

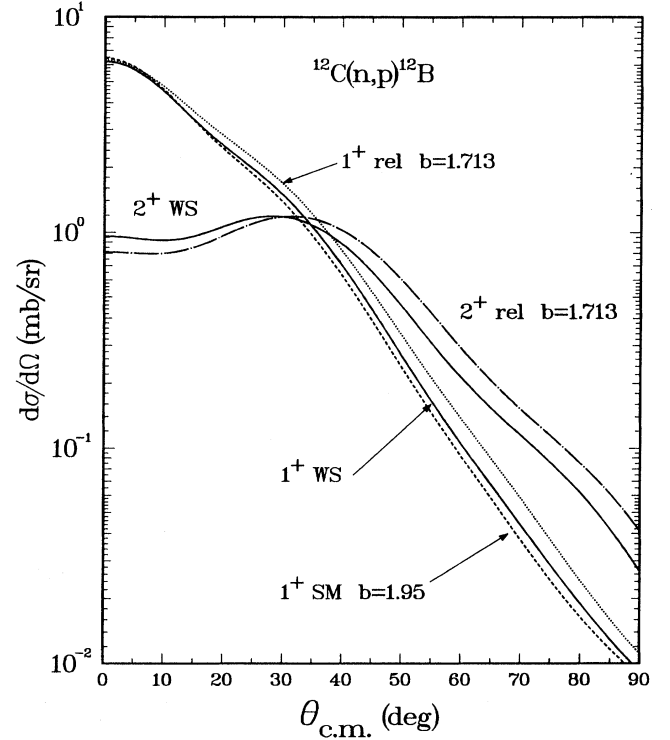


FIG. 5. DWBA cross sections for the $^{12}\text{C}(n,p)^{12}\text{B}$ reaction at 65 MeV for the first 1^+ and 2^+ $T=1$ levels using the Cohen and Kurath (Ref. 9) CK(POT) OBDME's and a variety of single-particle wave functions. For the curves labeled "rel," the relative coordinate OBDME's of Table I were used.

diffusivity at $a=0.65$ fm, set the spin-orbit potential to zero, and follow the well-depth prescription used by Millener *et al.*⁴⁰ to fit the rms charge radius of ^{12}C and obtain $r_0=1.41$ fm. Using the same value of r_0 for neutrons and protons gives, as expected, similar neutron and proton radii. Since the p -shell pickup strength from ^{12}C is concentrated⁴⁸ in the ground and first excited states of the $A=11$ core, we assume that the neutron in the final state is bound to the $A=11$ ground state if a $p_{3/2}$ proton makes the transition and to the $\frac{1}{2}^-$ state at about 2 MeV in the case of a $p_{1/2}$ proton. This saves us having to make the full core-state decomposition⁴⁰ of the one-body density-matrix elements. Thus, for a $p_{3/2}\rightarrow p_{1/2}$ transition to the ^{12}B ground state, the $p_{3/2}$ proton is bound by 15.96 MeV and the $p_{1/2}$ neutron by 3.37 MeV and so on. We take the binding energy for a $0s_{1/2}$ proton to be 34 MeV, although the precise value is not important.

Cross sections at 65 MeV to the ^{12}B ground state are displayed in Fig. 5 for two different oscillator parameters and for the Woods-Saxon (WS) case just described. The close agreement between the 0° cross sections for WS and harmonic-oscillator (HO) wave functions is a coincidence due to the offsetting tendencies of increased WS tails and lack of overlap between initial- and final-state radial wave functions. If all single-particle states are deeply bound at 16 MeV, the 0° cross section increases slightly to match almost exactly the HO value, while loosely binding all states at 2 MeV gives a 9% increase. For higher-

momentum transfers, the cross section naturally falls more rapidly for larger oscillator parameters. The cross section for WS wave functions is actually quite similar to that obtained when the oscillator parameter is chosen^{47,49} to fit best the shape of the (e,e') transverse form factor for the analog 1^+ state in ^{12}C . Effects due to the use of different radial wave functions are also evident in Fig. 5 for the cross sections to the 2^+ first excited state.

To aid our understanding of the cross sections presented in Fig. 5 in terms of the underlying nuclear structure, we give in Figs. 6 and 7 the cross sections for pure $\Delta L, \Delta S$ excitations (the unit LS OBDME's are transformed to jj coupling for input to DW81). Clearly, for the Cohen-Kurath wave functions, the $\Delta L=0, \Delta S=1$ amplitude dominates in the excitation of the 1^+ state and the effect of the $\Delta L=2, \Delta S=1$ amplitude is to put a small shoulder at around 30° in the angular distribution shown in Fig. 5. In the case of the 2^+ state, the $\Delta L=2, \Delta S=0$ and $\Delta L=2, \Delta S=1$ amplitudes are comparable in size for the Cohen-Kurath calculation. Empirical renormalizations of the Cohen-Kurath amplitudes, attributable in the main to core-polarization effects, are necessary to account for the measured electron-scattering form factors of the 1^+ and 2^+ levels. These effects are discussed later when we compare experiment and theory for the $^{12}\text{C}(n,p)^{12}\text{B}$ reaction.

In Fig. 8 we show cross sections at 65 MeV to 1^- states for pure $SU(3)$ excitations. Clearly, the cross sec-

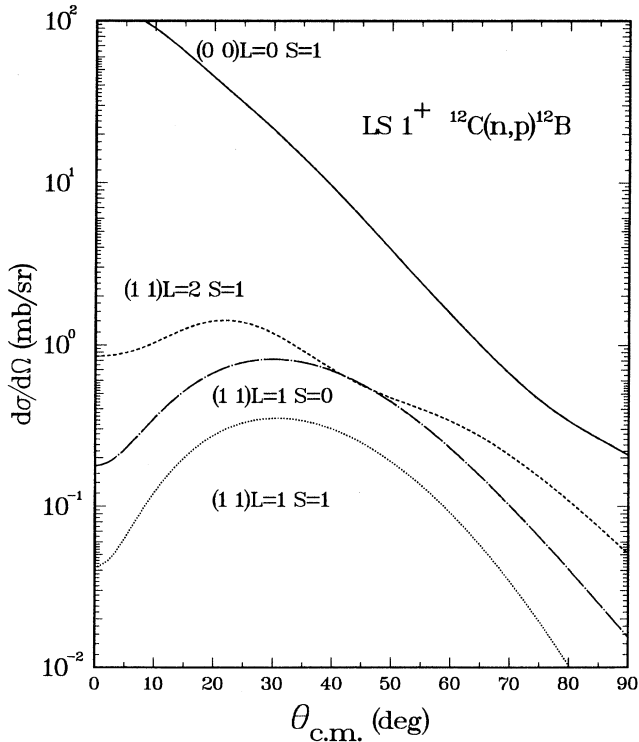


FIG. 6. Pure LS DWBA cross sections for a 1^+ final state in the $^{12}\text{C}(n,p)^{12}\text{B}$ reaction at 65 MeV. Harmonic-oscillator wave functions with $b=1.713$ fm were used.

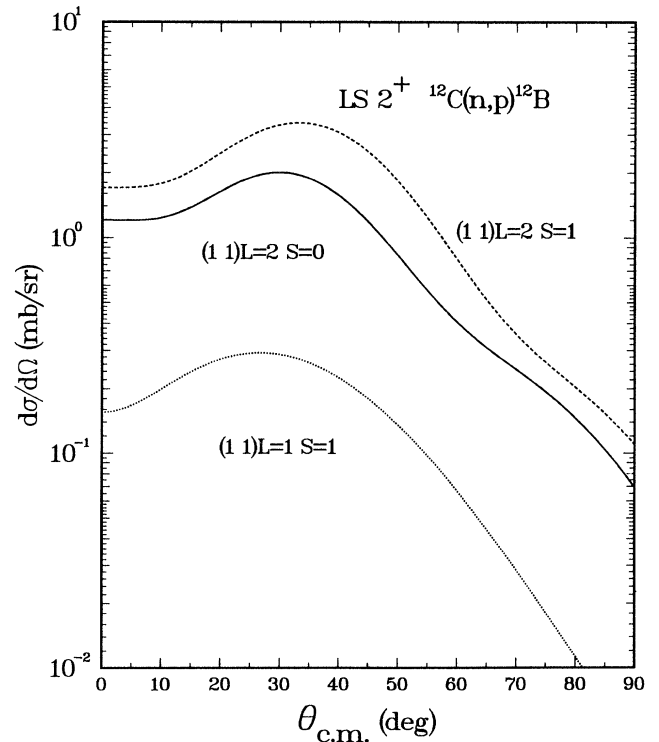


FIG. 7. Pure LS DWBA cross sections for a 2^+ final state in the $^{12}\text{C}(n,p)^{12}\text{B}$ reaction at 65 MeV. Harmonic-oscillator wave functions with $b=1.713$ fm were used.

tions are largest for $(\lambda\mu)=(10)$, which means that the quantity B , defined in Eq. (1), is indeed a useful measure of both the dipole and spin-dipole cross sections. Furthermore, the M3Y interaction³⁷ gives almost identical cross sections for $\Delta S=0$ and 1 so that, in either case,

$$\frac{d\sigma}{d\Omega}(18^\circ) \sim 0.74B \text{ mb/sr}, \quad (3)$$

where $b=1.64$ fm is used to evaluate B in Eq. (2). The corresponding cross sections for 2^- states, shown in Fig. 9, exhibit similar features. The (10) amplitude is dominant with a proportionality constant of 0.68 relating the 18° cross section to B . For the 0^- cross sections in Fig. 10, we show, in addition, the role played by the tensor force. Finally, to complete our breakdown of the contributions to the cross sections of negative-parity states, we show results for 3^- and 4^- states in Fig. 11. To illustrate how the information in Figs. 8–11 applies to the low-lying negative-parity states, we give in Table III OBDME's in the SU(3) representation for the states listed in Table II. The OBDME's are given in the conventional shell-model form, which is quite sufficient for qualitative comparisons. They can be transformed to the relative coordinate form, and the results in Table II recovered, using the prescription outlined in the Appendix. Further discussion of SU(3) form factors and transition densities can be found in Refs. 50 and 51.

To illustrate the effect of using Woods-Saxon wave functions on the cross sections for negative-parity states,

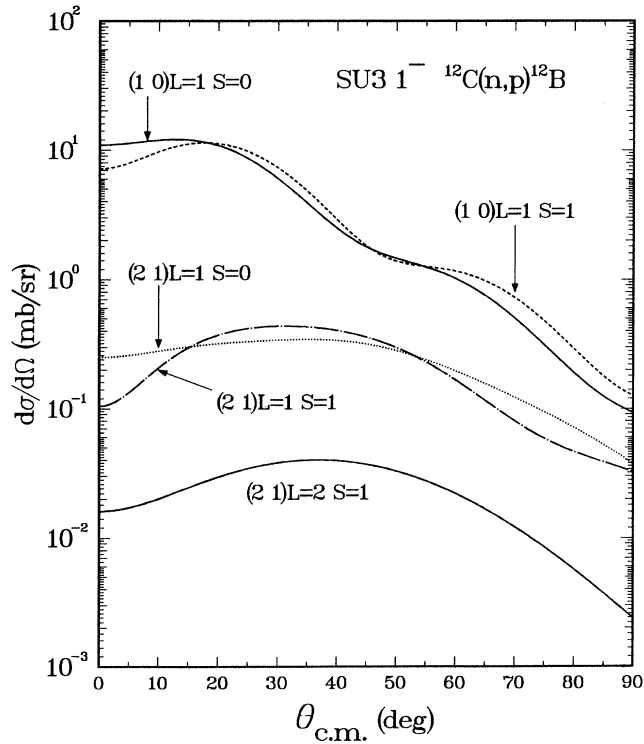


FIG. 8. Pure SU(3) DWBA cross sections for a 1^- final state in the $^{12}\text{C}(n,p)^{12}\text{B}$ reaction at 65 MeV. Harmonic-oscillator wave functions with $b=1.713$ fm were used.

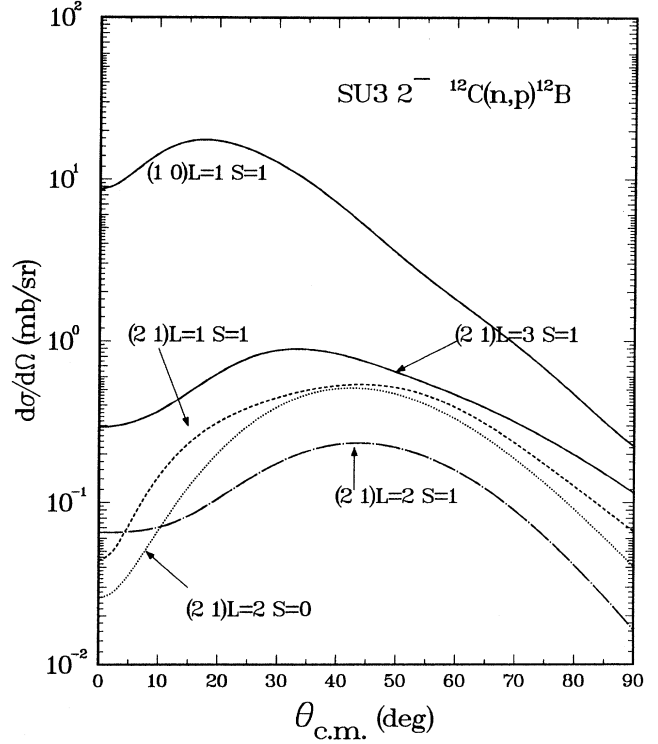


FIG. 9. Pure SU(3) DWBA cross sections for a 2^- final state in the $^{12}\text{C}(n,p)^{12}\text{B}$ reaction at 65 MeV. Harmonic-oscillator wave functions with $b=1.713$ fm were used.

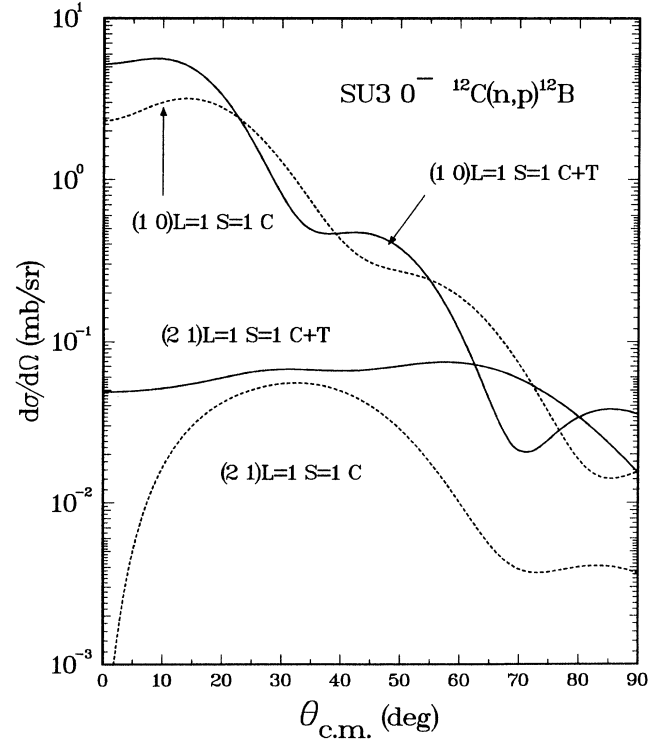


FIG. 10. Pure SU(3) DWBA cross sections for a 0^- final state in the $^{12}\text{C}(n,p)^{12}\text{B}$ reaction at 65 MeV. Harmonic-oscillator wave functions with $b=1.713$ fm were used. The cross sections for the purely central part of the M3Y interaction are shown as dotted curves.

we follow Clausen, Peterson, and Lindgren⁵² and calculate the cross section for an $M4$ excitation as a function of the binding energy of the $d_{5/2}$ neutron, the binding energy of the $p_{3/2}$ proton being fixed at 15.96 MeV. Using DW81,³⁵ we can follow the cross section across zero binding as long as the resonant state has a small width. The resultant peak cross sections are shown in Fig. 12 for binding energies ranging from 4 MeV bound to ~ 1 MeV unbound. For the 4^- state at 4.5 MeV, the $d_{5/2}$ neutron is unbound by 1.1 MeV, at which point the cross section has fallen to $\sim 70\%$ of the value for harmonic-oscillator wave functions. Similar reductions of peak cross sections also occur for the strong dipole excitations. For example, Fig. 13 shows a very similar reduction for the second 2^- level, which is almost degenerate with the 4^- level at 4.5 MeV. A different behavior is apparent for the excitation of the first 2^- level where a destructive interference between $p \rightarrow 1s$ and $p \rightarrow d$ contributions is involved. We cannot reliably follow the cross sections into the region of the giant dipole resonance since the final-state neutron is several MeV unbound. At this point a proper continuum shell-model treatment is called for.

In summary, we have, in this section, isolated the major contributions to the charge-exchange cross sections and shown that the use of single-particle wave functions more realistic than harmonic-oscillator wave functions can lead to appreciable changes in the predicted cross

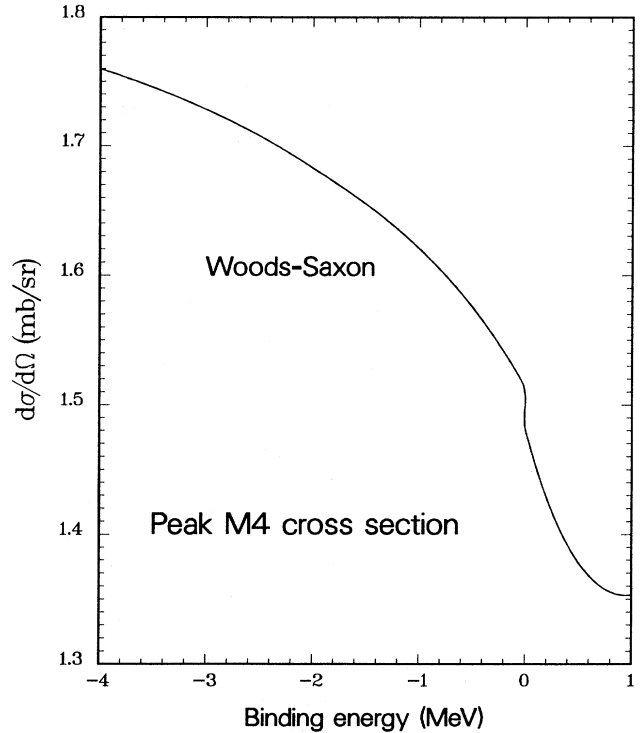


FIG. 12. Peak $M4$ cross sections for the $^{12}\text{C}(n,p)^{12}\text{B}$ reaction at 65 MeV as a function of the binding energy of the $d_{5/2}$ neutron in a Woods-Saxon well. The peak cross section for harmonic-oscillator wave functions with $b=1.713$ fm is 1.9 mb/sr and increases with increasing b .

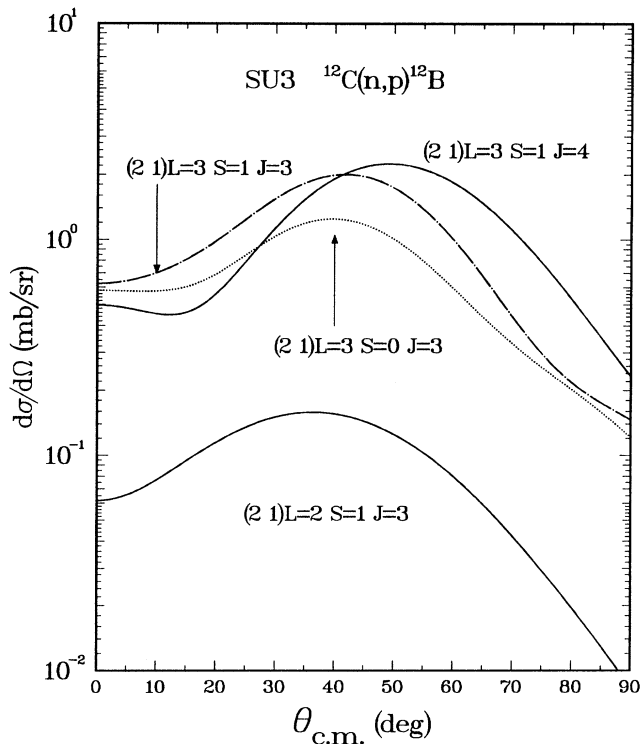


FIG. 11. Pure SU(3) (same as LS) DWBA cross sections for 3^- and 4^- final states in the $^{12}\text{C}(n,p)^{12}\text{B}$ reaction at 65 MeV. Harmonic-oscillator wave functions with $b=1.713$ fm were used.

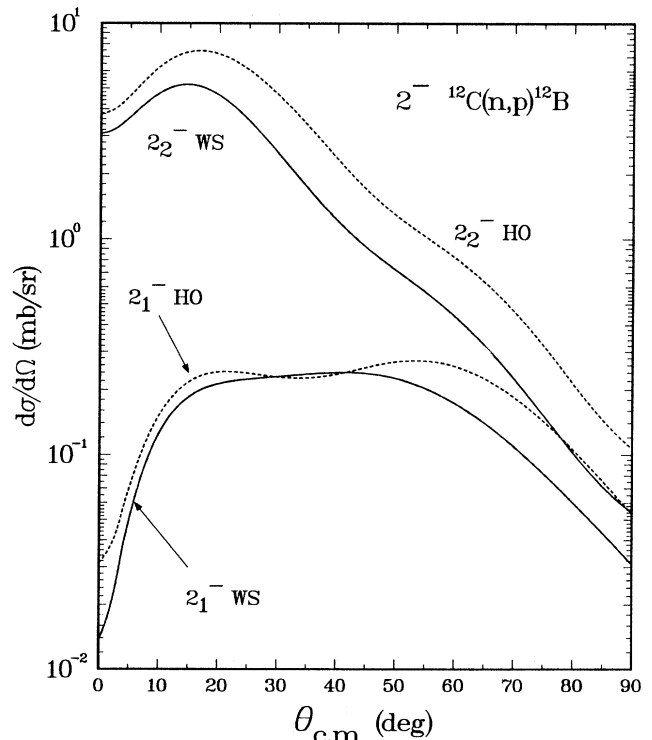


FIG. 13. Comparison of $^{12}\text{C}(n,p)^{12}\text{B}$ cross sections at 65 MeV for the two lowest 2^- shell-model states using harmonic-oscillator and Woods-Saxon wave functions.

TABLE III. Isovector one-body density-matrix elements^a in the SU(3) representation for negative-parity transitions.

| J_n^π | E_x (MeV) ^b | 1s0d-0p(21) | | | | 1s0d-0p(10) | | 0p-0s(10) | |
|-----------|--------------------------|--------------|-----------------------|---------------------|-----------------------|--------------|--------------|--------------|--------------|
| | | $\Delta S=0$ | $\Delta L=\Delta J-1$ | $\Delta L=\Delta J$ | $\Delta L=\Delta J+1$ | $\Delta S=0$ | $\Delta S=1$ | $\Delta S=0$ | $\Delta S=1$ |
| 0_1^- | 4.85 | | | | -0.5179 | | -0.2294 | | 0.0537 |
| 0_2^- | 9.29 | | | | -0.1811 | | 0.6513 | | 0.0374 |
| 0_3^- | 10.16 | | | | 0.0015 | | -0.0522 | | 0.3058 |
| 0_4^- | 14.49 | | | | 0.2300 | | -0.3866 | | -0.2980 |
| 1_1^- | 3.51 | 0.5460 | | -0.4536 | 0.1341 | 0.0618 | -0.2147 | 0.0677 | -0.0552 |
| 1_2^- | 5.38 | 0.3674 | | 0.3630 | 0.0126 | 0.1146 | 0.1103 | -0.0013 | -0.0356 |
| 1_3^- | 7.56 | 0.1653 | | 0.0860 | 0.2184 | -0.6128 | 0.0035 | -0.0275 | 0.0215 |
| 1_4^- | 8.34 | 0.1066 | | -0.2181 | -0.1008 | 0.2800 | 0.5566 | -0.0112 | -0.0295 |
| 1_5^- | 9.08 | 0.1989 | | -0.0497 | -0.2188 | 0.1952 | -0.3404 | 0.0205 | -0.0651 |
| 2_1^- | 2.75 | 0.2264 | -0.7381 | 0.1021 | 0.0972 | | -0.0835 | | 0.0133 |
| 2_2^- | 4.51 | 0.2787 | 0.0697 | -0.0769 | 0.1493 | | 0.6312 | | -0.0074 |
| 2_3^- | 6.52 | 0.3989 | 0.1910 | -0.0612 | 0.4492 | | -0.1587 | | -0.0063 |
| 2_4^- | 7.27 | -0.1636 | -0.1855 | -0.4850 | 0.1086 | | -0.3351 | | 0.0039 |
| 2_5^- | 8.48 | -0.2192 | 0.0312 | -0.0229 | 0.1762 | | 0.0191 | | 0.0446 |
| 4_1^- | 4.52 | | | | 0.8069 | | | | |

^aConventional shell-model OBDME's, which, for some of the states, can be transformed into those to be found in Table III of Ref. 12.

^bTheoretical excitation energies.

sections. Similar conclusions have been reached by Ohnuma *et al.*⁵³ in a systematic study of the factors which influence DWBA cross sections for the $^{12}\text{C}(p,n)^{12}\text{N}$ reaction at 35 and 40 MeV. Since a p -shell proton in the initial state or an sd -shell neutron in the final state possesses a large fraction of single-particle strength and is bound close to the energy expected for the orbit in the average field (Hartree-Fock energy), the Woods-Saxon wave functions obtained by the well-depth prescription should provide a good approximation to the required single-nucleon overlap functions. On the other hand, for the 1^+ and 2^+ states, the loosely bound p -shell neutron in the final state has only a small fraction of its parentage to the ^{11}B ground state and its separation energy is far from the Hartree-Fock energy. In this case the single-nucleon overlap function should be larger inside the nucleus than the Woods-Saxon wave function obtained by the well-depth prescription,⁵⁴ which will consequently underestimate the overlap between the initial- and final-state wave functions in the DWBA form factor.

IV. COMPARISON BETWEEN EXPERIMENT AND THEORY

A. Ground and 0.95-MeV states

As outlined in Sec. III B, our starting point for describing the structure of the lowest 1^+ and 2^+ levels is the p -shell model of Cohen and Kurath (CK).⁹ First, we investigate how well these wave functions describe the β decay of ^{12}B to the ^{12}C ground state and the electron-scattering form factors for the analog states in ^{12}C . Then we show that adjustments to the CK OBDME's can produce good fits to the form factors up to $q \sim 1.5 \text{ fm}^{-1}$ and use the resultant transition densities in DWBA calculations for the (n,p) reaction.

For the β decay of ^{12}B to the ^{12}C ground state, we have

$$g_A^2 B_{\text{GT}}(1^+ \rightarrow 0^+) = \frac{6166}{ft_{1/2}}. \quad (4)$$

In terms of the standard LS OBDME's, $O^{\Delta L \Delta S}$, with ^{12}C as the initial state,

$$B_{\text{GT}}^{1/2}(1^+ \rightarrow 0^+) = \sqrt{6} O^{01}. \quad (5)$$

Using $\log ft_{1/2} = 4.072$ and $g_A(\text{free}) = 1.26$, we find $O^{01} = 0.234$, which is close to either of the Cohen and Kurath values listed in Table IV. However, the well-known quenching of Gamow-Teller β -decay rates can be roughly described by taking $g_A(\text{eff}) \sim 1$, which suggests that O^{01} should be larger than the CK value.

When harmonic-oscillator wave functions are used, the transverse form factor for the electroexcitation of the 15.11-MeV 1^+ , $T=1$ state in ^{12}C can be written

$$F_T = q \frac{\sqrt{8\pi}}{3Z} f_{\text{SN}} f_{\text{c.m.}} e^{-y(a+by+cy^2+dy^3+\dots)}, \quad (6)$$

where $y = (bq/2)^2$, $f_{\text{c.m.}} = e^{y/A}$, and f_{SN} is the single-nucleon form factor. Up to cubic terms in the polynomial are required to fit the (e, e') data⁵⁵⁻⁵⁷ up to $q \sim 3 \text{ fm}^{-1}$. However, in a p -shell model only a and b are nonzero with

$$a = \mu_B \sqrt{9/8\pi} (-4O^{10} g_i^{(1)} - \sqrt{6} O^{01} g_s^{(1)}), \quad (7)$$

$$b = \mu_B \sqrt{3/5\pi} (\sqrt{5} O^{01} g_s^{(1)} - O^{21} g_s^{(1)}), \quad (8)$$

where $\mu_B = \hbar/2m_p c = 0.10515 \text{ fm}$, $g_i^{(1)}(\text{free}) = 0.5$, and $g_s^{(1)}(\text{free}) = 4.706$ (the superscript refers to ΔT). Then $BM1(0^+ \rightarrow 1^+) = a^2 \text{ fm}^2$ or $8\pi a^2 / (45\mu_B^2)$ W.u. The ground-state radiative width⁵⁵ of 38.5(8) eV implies $|a| = 0.179(2) \text{ fm}$, while the CK(POT) OBDME's in Table IV give, with the free-nucleon g factors, $a = -0.160$ [with contributions of 0.0041 and -0.1641 from the two terms in Eq. (7)]. This suggests that, as did the β -decay data, O^{01} should be larger than the CK

TABLE IV. Isovector LS one-body density-matrix elements for $^{12}\text{C}(\text{g.s.}) \rightarrow ^{12}\text{C}(15.11 \text{ MeV})$.

| Interaction | $\Delta L \Delta S$ | | | |
|----------------------|---------------------|-----------|----------|----------|
| | 01 | 10 | 11 | 21 |
| CK(POT) ^a | 0.226 21 | -0.032 66 | 0.727 99 | 0.136 14 |
| CK(816) ^a | 0.235 03 | -0.026 02 | 0.719 60 | 0.151 95 |
| Fit ^b | 0.248 70 | c | c | 0.042 30 |
| MP4 ^d | 0.288 65 | -0.097 35 | 0.765 90 | 0.168 13 |
| MP4F ^e | 0.295 00 | f | f | 0.050 00 |

^aReference 9.

^bA fit up to $q = 1.79 \text{ fm}^{-1}$ to F_T^2 from Ref. 55 gives, for the parameters in Eq. (6), $a = -0.1760(12) \text{ fm}$, $b = 0.1109(13) \text{ fm}$, and $b_0 = 1.822(12) \text{ fm}$, where b_0 is the oscillator parameter. Equations (7) and (8) are used to obtain O^{01} and O^{21} after O^{11} (which does not enter) and O^{10} (which makes a small contribution to a) are fixed at the CK(POT) values.

^cFixed at CK(POT) value.

^dFrom an empirical fit to energy-level data for $A = 10-16$.

^e O^{01} and O^{21} are adjusted to fit F_T^2 up to $q \sim 1.8 \text{ fm}^{-1}$ when Woods-Saxon wave functions ($r_0 = 1.41 \text{ fm}$) are used. An even better fit is obtained for $r_0 = 1.35 \text{ fm}$, which moves the minimum to slightly higher q .

^fFixed at MP4 value.

value, particularly since $g_s^{(1)}(\text{eff})$ obtained from fits to $M1$ data⁵⁸ or theoretically^{59,60} is less than $g_s^{(1)}(\text{free})$ with a typical value of ~ 4 . The CK(POT) interaction gives $b = 0.080 \text{ fm}$, with contributions of 0.1094 and -0.0294 from O^{01} and O^{21} , respectively, in Eq. (8). As can be seen from Fig. 14, the CK wave functions produce a minimum at too high a momentum transfer and seriously underestimate the second maximum of the $M1$ form factor. The minimum can be moved in by reducing O^{21} , as suggested by core-polarization calculations,⁶¹ and a good fit to F_T^2 can be obtained up to $q \sim 1.8 \text{ fm}^{-1}$. The OBDME's from fits with HO and WS wave functions are given in Table IV (see the footnotes for details), and the resultant form factor for WS wave functions is shown in Fig. 14. For the same OBDME's, HO and WS wave functions give rather different magnitudes at the first maximum, reflecting the lack of overlap of the WS single-particle wave functions in the initial and final states; the single-nucleon overlap function in the final state will, as noted in Sec. III C, differ from either the HO or WS wave function.

The longitudinal^{62,63} and transverse^{57,62} form factors for the 16.11-MeV 2^+ , $T=1$ level are shown in Fig. 15. The curves are obtained using the CK OBDME's, WS wave functions $1 + \delta e_p - \delta e_n = 0.577$ and $g_s^{(1)} = 0.915 g_s^{(1)}(\text{free})$. We note that WS wave functions reproduce the shape of the longitudinal form factor at low q very well, in the sense that the BC2 value and the magnitude of the peak of the form factor are simultaneously reproduced; to do the same with HO wave functions requires a very large value of b and a smaller effective charge (cf. Fig. 5 of Ref. 62).

The form factors discussed above are determined mainly by the same OBDME's (O^{01} for $M1$, O^{20} for $C2$, and O^{21} for $E2$) which are most important for the $^{12}\text{C}(n,p)^{12}\text{B}$ cross sections (see Figs. 6 and 7). Therefore, we use the renormalized OBDME's, which fit the (e, e') data up to $q \sim 1.5 \text{ fm}^{-1}$, to compute the (n, p) cross sections.

Figure 16 shows the cross sections, plotted against

momentum transfer q , for the ground state plus 0.95-MeV excitation ($0^+ \rightarrow 1^+$ plus $0^+ \rightarrow 2^+$ transitions) for the present data and 56.3-MeV data.³ Also shown are data for the 0.95-MeV excitation at 60 MeV. Agreement among the different data sets is generally good. DWBA

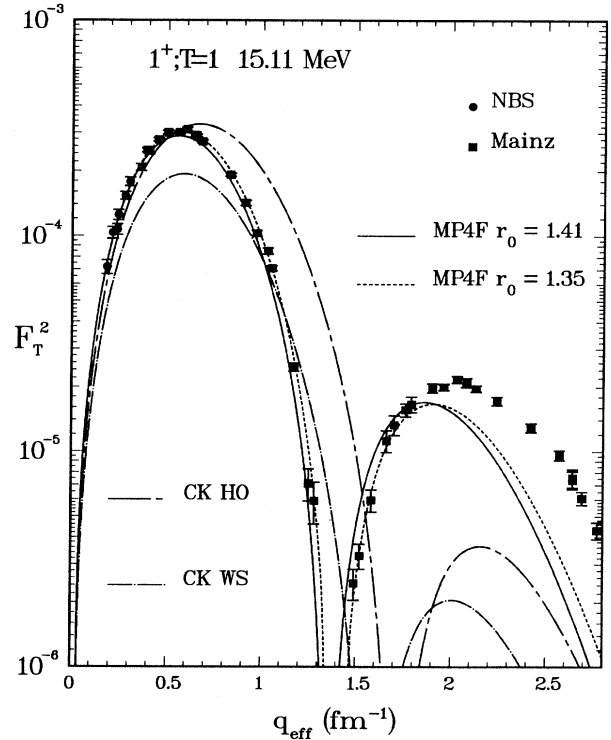


FIG. 14. Transverse (e, e') form factors for the excitation of the 15.11-MeV 1^+ , $T=1$ level of ^{12}C . The Mainz data are from Ref. 55, which includes a reanalysis of the older NBS data of Ref. 56. The University of Massachusetts data of Ref. 57 are in good agreement with the Mainz data and extend to $q = 4 \text{ fm}^{-1}$. The OBDME's are from Table III (see footnotes) and the relative oscillator parameter has the value $b = 1.713 \text{ fm}$.

predictions at 65 MeV for the ground state plus 0.95-MeV excitation and for the 0.95-MeV excitation alone are also shown. These have good overall agreement with the data up to $q \approx 300 \text{ MeV}/c$ ($\approx 60^\circ$ c.m. angle), which is within the limits of reliability of the renormalized p -shell transition densities. The lower curves for each state include the central and spin-orbit parts of the effective interaction, while the upper curve includes the tensor, central, and spin-orbit parts (the spin-orbit contribution is negligible). The tensor part is clearly needed to reproduce the data. If we normalize to the β -decay rate ($O^{01}=0.234$), assuming that core-polarization effects dominate in the quenching of Gamow-Teller matrix elements,^{58–60} and use HO wave functions (perfect overlap), a normalization factor or ~ 0.65 is required. In Sec. V we attribute the need for this renormalization factor to a well-known deficiency of the M3Y interaction. If the set of OBDME's labeled MP4F from Table IV are used, a larger reduction factor of 0.44 is required because a large value for O^{01} was used in fitting the $M1$ form factor (see Fig. 14 and Table IV) to compensate for the lack of overlap of WS wave functions. The (n,p) cross section for the 2^+ state is not determined well enough to make any strong statement concerning normalization factors.

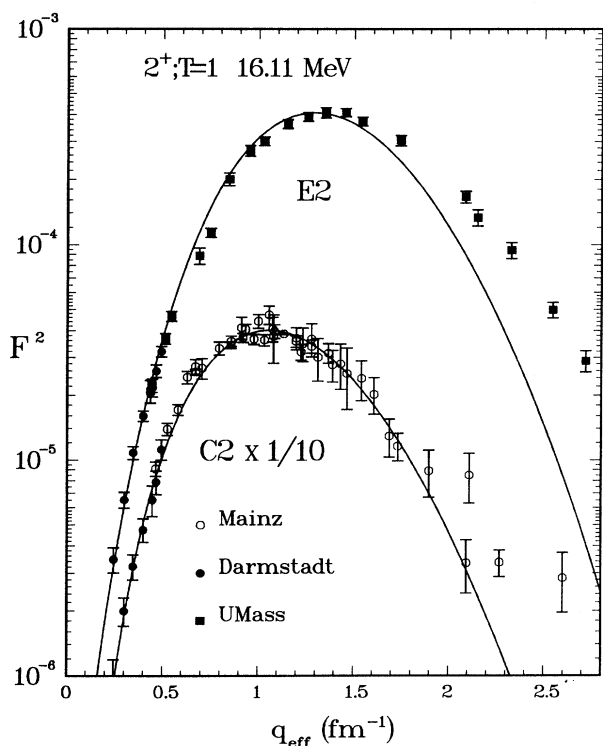


FIG. 15. Longitudinal and transverse (e, e') form factors for the excitation of the 16.11-MeV 2^+ , $T=1$ level of ^{12}C . The data are from the University of Massachusetts (Ref. 57), Darmstadt (Ref. 62), and Mainz (Ref. 63). The curves are generated using Woods-Saxon wave functions ($r_0=1.41 \text{ fm}$), $1+\delta e_p - \delta e_n = 0.577$, and $g_s^{(1)}=4.306$. The continuity equation is used in obtaining the $E2$ form factor [see Eq. (15) of Ref. 41].

However, (p, n) and (p, p') data at 62 MeV (Refs. 23 and 24) and (p, p') data at 65 MeV (Ref. 64) (see Fig. 19) indicate that the peak (n, p) cross section should be 0.6 mb/sr, which is slightly below the DWBA curve in Fig. 16.

B. Negative-parity states near 4.4 MeV excitation energy

The $^{12}\text{C}(n, p)^{12}\text{B}$ differential cross section data for the 4.4-MeV peak are shown in Fig. 17. There were some difficulties with the 60-MeV data, particularly for the 4.4-MeV structure. To begin with, the data (Fig. 2) do not have high statistical accuracy. The dipole region cross sections at 60 MeV are on average ($\approx 10\%$) below those at the other two energies. However, the 4.4-MeV cross sections at some angles are as much as 30% below those at the other two energies, for which the data sets agree quite well. Although we cannot explain such large discrepancies, we decided to exclude the 4.4-MeV cross sections from Fig. 17. Previously,² a macroscopic model

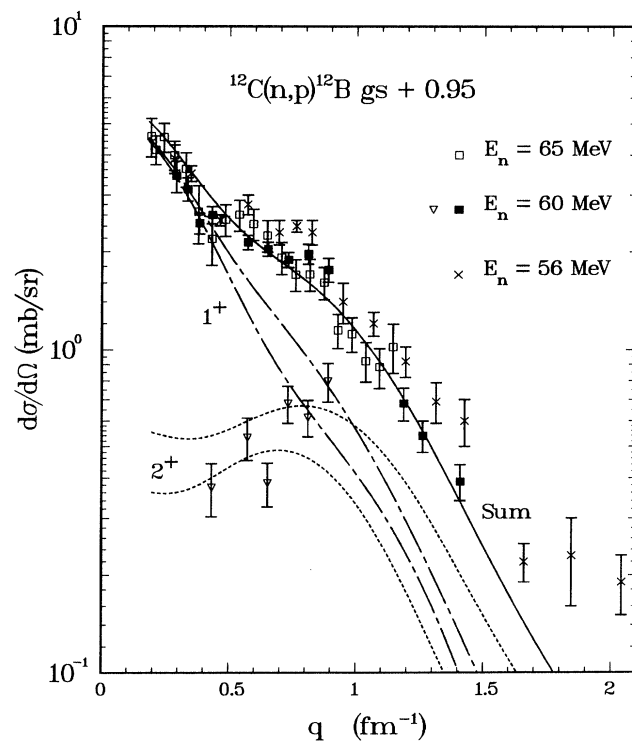


FIG. 16. Differential cross sections for the unresolved ground and first excited states of ^{12}B from the $^{12}\text{C}(n, p)^{12}\text{B}$ reaction at 56.3, 60, and 65 MeV incident energy. A few points are shown for the 0.95-MeV 2^+ state from the 60-MeV data. Also shown are the results of microscopic DWBA calculations at 65 MeV using the full M3Y effective interaction and p -shell transition densities adjusted to fit electron-scattering data. The lower curves for each state show the cross sections when only the central and spin-orbit parts of the effective N - N interaction are included, while the upper curves include the effects of the tensor force. The normalization factor for the 1^+ state is discussed in the text.

was used to fit the 56-MeV data and the angular distribution was well reproduced by a superposition of $L=1$ and 3, in line with presence of a 2^- state at 4.37 MeV and a 4^- state at 4.54 MeV according to the $^{11}\text{B}(n,n)^{11}\text{B}$ data of Lane *et al.*⁶⁵ In fact, the predominant contributor to this peak, or the analog 19.5-MeV complex in ^{12}C , in a variety of reactions at low-momentum transfer is the broad 2^- level at ~ 4.4 MeV. At high-momentum transfer, the 4^- level at 4.52 MeV is most strongly excited. The roles of the two states are clearly exhibited in the $^{12}\text{C}(e,e')^{12}\text{C}$ reaction,¹² the $^{12}\text{C}(e,e'\pi^+)^{12}\text{B}$ reaction,⁶⁶ and the $^{12}\text{C}(\gamma,\pi^+)^{12}\text{B}$ reaction,²¹ while the 2^- state dominates in the $^{12}\text{C}(\pi^-, \gamma)^{12}\text{B}$ reaction.²⁰ For the nuclear-structure model used here ($0\hbar\omega$ initial state and $1\hbar\omega$ final state), normalization factors of ~ 0.3 and ~ 0.7 are typically required for the $M2$ and $M4$ cross sections if HO wave functions are used.^{12,66,67} The DWBA cross sections shown in Fig. 17 use Woods-Saxon wave functions (unbound at the physical separation energy of ~ 1 MeV for the $d_{5/2}$ neutron orbit) which reduce the cross sections below the HO values by roughly 30% (depending somewhat on the choice of well parameters). Normalization factors of 0.53 and 1.0 were used for the 2^- and 4^-

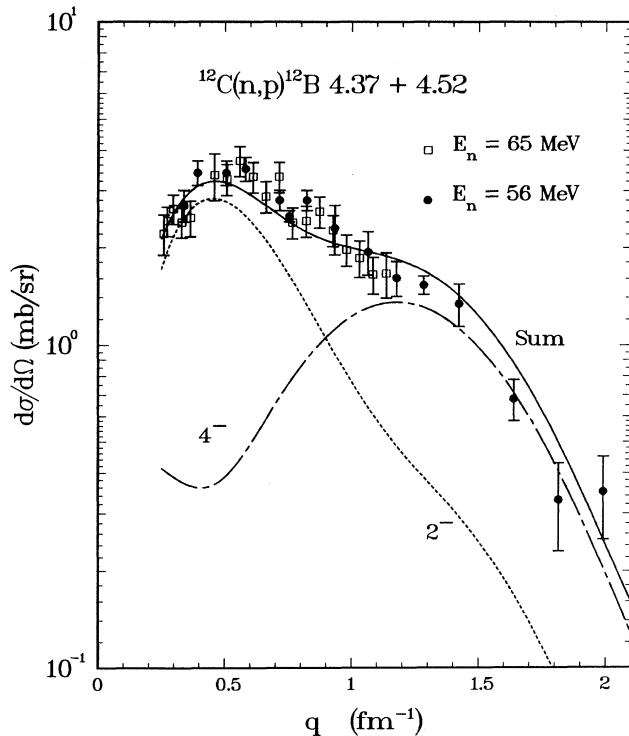


FIG. 17. Differential cross sections for the 4.4-MeV peak in the $^{12}\text{C}(n,p)^{12}\text{B}$ reaction at 56.3 and 65 MeV incident energy. The main contributions to the peak are assumed to be from the 2^- and 4^- states at 4.37 and 4.52 MeV excitation energy, respectively. The DWBA curves are calculated for Woods-Saxon wave functions with the $d_{5/2}$ neutron unbound at the physical separation energy from the ^{11}B ground state and the $s_{1/2}$ neutron bound by 300 keV. A normalization factor of 0.53 has been applied to the 2^- cross section.

states. For these states the effect of using Woods-Saxon wave functions is similar for electron-scattering form factors and (n,p) cross sections. We note that the exploratory calculations with Woods-Saxon wave functions made by Hicks *et al.*¹² used sd orbits bound by 2 MeV (and $r_0=1.25$ fm) and did not show dramatic differences from calculations with HO wave functions. According to Sagawa and Brown,⁴³ the 2^- cross section is expected to be further reduced 25% by ground-state correlations and a normalization factor of 0.71, which is close to the factor 0.65 for the 1^+ state, would be required.

The wave functions of the low-lying negative-parity states of ^{12}B are rather simply expressed¹² in terms of an $s_{1/2}$ or $d_{5/2}$ neutron coupled to the low-lying states of ^{11}B . In particular, the dominant component in the 2_1^- state at 1.67 MeV is $^{11}\text{B}(\text{g.s.}) \otimes s_{1/2}$ with an appreciable admixture of $^{11}\text{B}(\text{g.s.}) \otimes d_{5/2}$ and vice versa for the 2_2^- state. The dominant OBDME's then have $\Delta L=1$ and $\Delta S=1$ with $(\lambda\mu)$ equal to (21) for the first state and (10) for the second (see Table III). Thus^{50,51} the form factor for the first state¹² peaks at high q and that for the second at low q . The HO form factor for the 2_1^- , $T=1$, 16.58-MeV state in ^{12}C required normalization by a factor of 0.65 to fit the (e,e') data.¹² The use of WS wave functions essentially reproduces the most recent (e,e') data^{55,57} without renormalization. We note that random-phase-approximation (RPA) correlations are not expected to strongly renormalize the (21) transition density. Since the $s_{1/2}$ orbit lies below the $d_{5/2}$ orbit in this mass region, the strong isovector $M2$ excitations in neighboring nuclei exhibit a similar behavior with respect to form-factor shape and energy separation.

C. Giant dipole resonance region

Figure 18 shows the measured differential cross section as a function of momentum transfer for the region of excitation energy in ^{12}B between 6.0 and 9.5 MeV compared to DWBA cross sections for the dipole and spin-dipole states predicted in the energy region. As can be seen from Fig. 4, the 1_3^- state at 7.6 MeV is excited by a pure dipole transition with $\Delta S=0$, while the 1^- states at 8.3 and 9.1 MeV are predominantly spin-dipole excitations. The shape of the $\Delta L=1$ angular distribution obtained by summing the cross sections for the three 1^- states provides an excellent description of the data. Although the 1^- states are expected to provide most of the (n,p) strength in the 6.0–9.5-MeV energy region, 2^- states predicted at 6.5 and 7.3 MeV and a 0^- state at 9.3 MeV carry some strength as shown in Fig. 18 where the DWBA cross sections for all six states have been multiplied by a common factor of 0.35 and then summed. There is some uncertainty as to which model states should be included in the comparison. If the 1_5^- and 0_2^- states predicted at the upper end of the energy range are omitted, a normalization factor of 0.46 is required. We recall that ground-state correlations reduce both the dipole and spin-dipole cross sections, by a factor of ~ 0.75 in the latter case according to Sagawa and Brown,⁴³ and thus account for part of the reduction. Also, the states considered have large parentages, particularly $d_{5/2}$ and $d_{3/2}$, to the ^{11}B

ground and low-lying excited states and consequently have large widths since they are unbound with respect to neutron emission by 3–6 MeV. The DWBA cross sections in Fig. 18 were obtained with the d orbits unbound by 1 MeV and the $1s$ orbit bound by 200 keV (as for the states in the 4.4-MeV peak). This is far as one can reasonably go on the basis of bound-state shell-model calculations, but one might expect a further reduction in cross section for the more unbound physical states.

The dominance of 1^- excitations in the giant resonance region is in agreement with the results of Sterrenburg *et al.*²⁵ who studied the angular correlations of decay protons following formation at 0° in the $^{12}\text{C}(^3\text{He},t)^{12}\text{N}$ reaction. In a region of excitation energy covering the main peak of the giant dipole resonance, their data was well fitted by 1^- excitation with $\sim 10\%$ admixture of 2^- . For comparison, the ratio of 0° cross sections for $2_3^- + 2_4^-$ to $1_3^- + 1_4^-$ is 0.16. Sterrenburg *et al.* also find that 0^- excitation is more important than 1^- excitation at the upper end of the energy region. This is in agreement the strength distributions shown in Fig. 4 and the DWBA results for the 1_5^- and 0_2^- model states shown in Fig. 18.

It is clear from Fig. 4 [equivalently, the $p \rightarrow sd(10)$ amplitudes of Table III] and the near equality of the $\Delta S = 0$

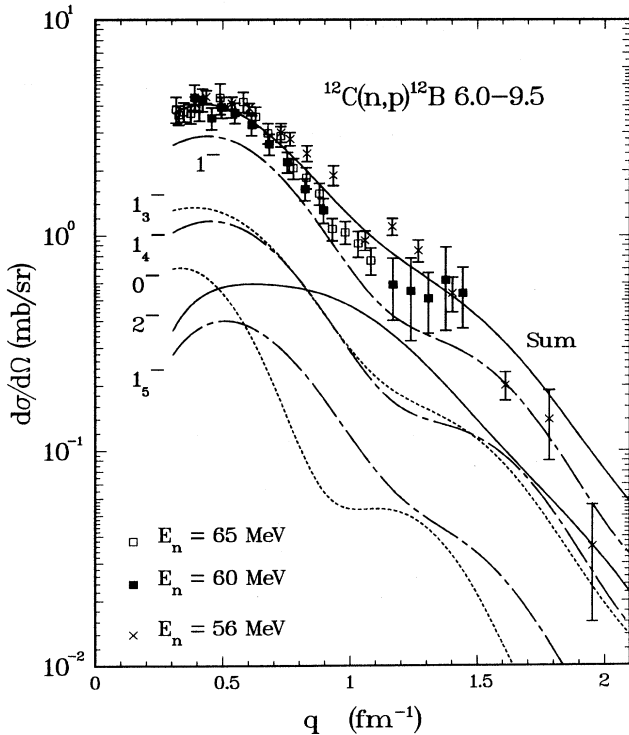


FIG. 18. Differential cross sections for the giant dipole resonance region in the $^{12}\text{C}(n,p)^{12}\text{B}$ reaction at 56.3, 60, and 65 MeV incident energy. DWBA curves are shown for three 1^- states, their sum, the sum of two 2^- states, and a 0^- state, all of which are predicted to lie in the 6.0–9.5-MeV region of excitation energy. All the calculated cross sections are multiplied by a factor of 0.35.

and 1 cross sections for $(\lambda\mu)=(10)$ in Fig. 8 that comparable contributions from spin-flip and non-spin-flip strength are expected in the giant resonance region for the $^{12}\text{C}(n,p)^{12}\text{B}$ reaction at 65 MeV. As the incident energy is increased, we would expect the $\Delta S=0$ excitation to become relatively less important on account of the well-known behavior⁶⁸ of the central t -matrix components with bombarding energy (see Table V). Gaarde *et al.*¹⁴ have given ratios at $\theta_{\text{c.m.}} \sim 5^\circ$ for the cross section of the 4-MeV relative to the 7-MeV structure in the $^{12}\text{C}(p,n)^{12}\text{N}$ reaction at 120, 160, and 200 MeV. They are listed in Table VI together with the corresponding quantity for the $^{12}\text{C}(n,p)^{12}\text{B}$ reaction at $\theta_{\text{c.m.}} \sim 18^\circ$ (ratio at peak for the 2^- curve in Fig. 17 and the sum curve in Fig. 18) and theoretical values at a selection of angles. The 4-MeV peak is assumed to be due to $\Delta S=1$ excitation of the 2_2^- state, with a correction made at 65 MeV for the excitation of the 4_1^- state (the 4^- cross section at small angles is negligible at the higher energies). In making comparisons between theory and experiment for quantities involving cross sections in the giant resonance region, it should be noted that there are always uncertainties associated with the subtraction of background from the experimental data. Also, the range of excitation energy over which the cross section is summed varies from experiment to experiment, making it more difficult to compare data from different experiments and to decide which model states should be included in the comparison. For the data of Gaarde *et al.*,¹⁴ no background subtraction was made and summation range was simply described as being over the 7-MeV peak. Accordingly, we give several theoretical ratios in Table VI. The agreement between theory and experiment in Table VI is quite good. We note that at low energies the ratio R_1 is considerably less than unity, while $R_1(\Delta S=1)$ is somewhat greater than unity, consistent with ratios measured in various photopion reactions,^{18,20,21} in which $\Delta S=1$ amplitudes are believed to dominate. In the same vein the 4-MeV peak is relatively more prominent in the $(d,^2\text{He})$ spectra^{15,17} and the (d,pn) spectrum.²⁷ We conclude that the available data are in qualitative agreement with the prediction that there is comparable dipole and spin-dipole strength in the giant resonance region.

TABLE V. Proportionality of peak DWBA cross sections to the quantity B of Eq. (1) for the $^{12}\text{C}(p,n)^{12}\text{N}$ reaction as a function of incident energy. At 65 MeV the M3Y interaction is used. At 120, 160, and 200 MeV, the 140-, 175-, and 210-MeV t matrices of Franey and Love (Ref. 69) were used with the optical potentials of Ref. 22. The angle at which the cross section peaks varies somewhat with multipolarity (see Figs. 8 and 9) and decreases with incident energy from $\sim 18^\circ$ for 65 MeV to a rough average of $\sim 12^\circ$ for the higher energies.

| Multipolarity | Incident energy (MeV) | | | |
|---------------|-----------------------|------|------|-------|
| | 65 | 120 | 160 | 200 |
| $M2$ | 0.69 | 0.50 | 0.54 | 0.56 |
| $E1$ | 0.74 | 0.75 | 0.73 | 0.73 |
| $C1$ | 0.78 | 0.23 | 0.14 | 0.095 |

V. (n, p) COMPARED WITH (p, n) AND (p, p')

Figure 19 shows a comparison of the summed cross sections for the lowest 1^+ and 2^+ $T=1$ states in the (n, p) , (p, p') , and (p, n) reactions on ^{12}C at 65, 65,⁶⁴ and 62,^{23,24} respectively. The agreement between the data sets when plotted against momentum transfer is within a range of about 10%. The corresponding DW81 cross sections are indistinguishable. Also shown in Fig. 19 are data points for the 2^+ state alone. The DWBA curves are the same as those shown in Fig. 16.

The (n, p) reaction, as does the (p, n) , selects the isovector parts of the effective NN interaction, and, for the particular case of Gamow-Teller transition with $\Delta L=0$ and $\Delta S=1$, a simple factorized expression for the cross section at low q , and at intermediate energies, has been derived:⁷⁰⁻⁷²

$$\frac{d\sigma}{d\Omega}(q, \omega) = K(E_n, \omega) N^D |J_{\sigma\tau}|^2 B_{\text{GT}}, \quad (9)$$

where

$$K(E_n, \omega) = \frac{E_i E_f}{(\pi \hbar^2 c^2)^2} \frac{k_f}{k_i},$$

N^D is the ratio of distorted- to plane-wave cross sections, $|J_{\sigma\tau}|$ is the volume integral (including exchange) of the corresponding central component of the NN interaction, and $B_{\text{GT}}(^{12}\text{C} \rightarrow ^{12}\text{B})$ is the Gamow-Teller (GT) transition strength⁷¹ derived from the β^- decay of ^{12}B [$B_{\text{GT}}(^{12}\text{C} \rightarrow ^{12}\text{B}) = 0.99$, from⁵ $\log ft(^{12}\text{B} \rightarrow ^{12}\text{C}) = 4.072$]. For the $^{12}\text{C}(n, p)^{12}\text{B}$ reaction at 0° and 65 MeV, the momentum transfer is 0.18 fm^{-1} and the energy loss ($\omega = E_x - Q_{\text{g.s.}}$) is 12.6 MeV. Recent investigations^{71,72} relate the β -decay strength to (p, n) cross sections extrapolated to zero energy and momentum transfer. To make this extrapolation, to evaluate N^D , and to get the value of $|J_{\sigma\tau}|$ for the M3Y interaction, we have run the DWBA code, with the Q value for the reaction set to zero, for a

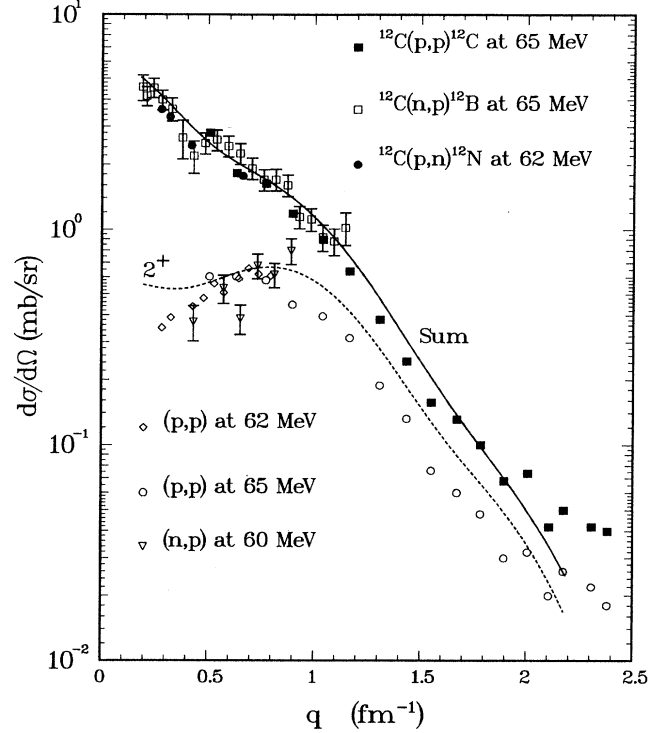


FIG. 19. Differential cross sections for the lowest 1^+ and 2^+ $T=1$ states in the $^{12}\text{C}(n, p)^{12}\text{B}$ (present data), $^{12}\text{C}(p, p')^{12}\text{C}$ (Refs. 23, 24, and 64), and $^{12}\text{C}(p, n)^{12}\text{N}$ (Refs. 23 and 24) reactions. The (p, p') cross sections have been multiplied by a factor of 2. The upper set of cross sections is the sum for the two states, while the lower set is for the 2^+ state alone. The DWBA curves are described in the caption to Fig. 16.

pure GT transition and HO wave functions with $b = 1.9 \text{ fm}$. Any errors inherent in this procedure are small compared with the uncertainties in the experimental cross sections. We find the distortion factor for $q = \omega = 0$ to be $N^D = 0.32$ and $|J_{\sigma\tau}| = 230 \text{ MeV fm}^3$ for the M3Y interac-

TABLE VI. Ratios for strengths of the 4.4- and 7.7-MeV peaks in the $^{12}\text{C}(p, n)^{12}\text{N}$ reaction at various incident energies and angles. The ratio R_1 refers to the calculated cross section for the 2_2^- model state divided by that for $1_3^- + 1_4^- + 2_3^- + 2_4^-$. The ratio R_2 includes in the denominator the contribution from the 1_5^- state. If ΔS is specified, only the contribution of that spin transfer is included in the denominator. The cross sections at 65 MeV were estimated using the pure SU(3) cross sections (HO wave functions) of Figs. 8 and 9 for the (n, p) reaction and the appropriate $(\lambda\mu) = (10)$ amplitudes from Table III (see also Fig. 4). Similar calculations were made for the higher incident energies (Table V can be used for $\theta_{\text{c.m.}} \sim 12^\circ$).

| Ratio | $\theta_{\text{c.m.}}$ | Incident energy (MeV) | | | |
|-------------------|------------------------|-----------------------|------|------|------|
| | | 65 | 120 | 160 | 200 |
| Expt. | 5° | 0.67 ^a | 0.64 | 0.76 | 0.84 |
| R_1 | 4° | 0.45 | 0.56 | 0.76 | 0.88 |
| | 6° | 0.49 | 0.62 | 0.82 | 0.93 |
| | 12° | 0.63 ^a | 0.72 | 0.88 | 0.96 |
| | 6° | | 0.51 | 0.67 | 0.76 |
| R_2 | 6° | | 0.51 | 0.67 | 0.76 |
| $R_1(\Delta S=1)$ | 12° | 1.18 ^a | 0.94 | 1.02 | 1.05 |
| $R_1(\Delta S=0)$ | 12° | 1.36 ^a | 3.07 | 5.84 | 9.30 |

^aFor peak cross sections at $\theta_{\text{c.m.}} \sim 18^\circ$.

tion, which is known^{38,73,74} to overestimate cross sections for our incident energies. We note that using the prescription of Love and Franey⁷⁵ to estimate an approximate value for $|J_{\sigma\tau}|$ yields 250 MeV fm^3 (cf. Fig. 7 of Ref. 73). The (n,p) cross section at 65 MeV for the unresolved 1^+ and 2^+ states is $4.6 \pm 0.6 \text{ mb/sr}$ at $q=0.19 \text{ fm}^{-1}$. From this value we subtract 0.4 mb/sr for the contribution from the 2^+ state, leaving 4.2 mb/sr , which is consistent with an extrapolation from the (p,n) data points at low q for the ^{12}N 1^+ state (see Fig. 19). The extrapolation to $q=\omega=0$ gives 5.9 mb/sr ($0.59 \text{ fm}^2/\text{sr}$). To reproduce this value we need $|J_{\sigma\tau}| \doteq 183 \text{ MeV fm}^3$, with a conservative error of 20%. Recently, the (n,p) reaction at energies between 60 and 260 MeV has been studied at Los Alamos for ^6Li , ^{12}C , and ^{13}C targets. The values of $|J_{\sigma\tau}|$ extracted⁷⁶ from the data at 12 energies are concordant for the three targets and decrease slowly from ~ 183 to $\sim 140 \text{ MeV fm}^3$ over the energy range in a manner consistent with the values given by recently developed t - and G -matrix interactions.⁶⁸

We would like to use these new interactions, but unfortunately, the exchange terms for the tensor components exhibit pathologies at low energies, in part because the NN data do not determine the interaction at the required momentum transfers.⁷⁷ The volume integral $|J_{\sigma\tau}|$ contains large contributions, for realistic interactions, from both even- and odd-state central components of the force, with the long-range one-pion-exchange (OPE) component contributing about 120 MeV fm^3 . The fact that the G -matrix interactions overestimate $|J_{\sigma\tau}|$ at energies near ours has led to suggestions that the odd-state components of the force be omitted.⁷⁸ However, it is unphysical to omit the OPE components.⁷⁹ For the odd-state components, an ambiguity associated with the addition of a δ function (a constant in momentum space) with arbitrary strength exists.^{79,80} This feature is well illustrated in Fig. 1 of Ref. 80, and we note that the singlet-odd component of the 50-MeV t matrix⁶⁹ is actually strongly attractive, providing another illustration of the same ambiguity.

Another interaction⁷⁴ which omits OPE in the odd-state central components (no triplet odd, ALTSO singlet odd³⁷) yields a 20% reduction in the 0^+ cross section for the ^{12}B ground state with $|J_{\sigma\tau}|=206 \text{ MeV fm}^3$. It is interesting to note that the calculated cross section for the 2^+ state is very little changed when this alternative interaction is used (even the contribution from the purely central part of the force is reduced by only 4%), thereby improving the calculated ratio of 1^+ to 2^+ cross sections, although both cross sections remain too large. For selected negative-parity states, there are reductions by factors of 0.87, 0.88, and 0.79 for the 2_2^- , 1_3^- , and 1_4^- states, respectively. Generally speaking, a reduction in the strength of the central force would much improve the agreement between the calculated and experimental cross sections in Figs. 16–19; only the 2^+ and 4^- states receive significant contributions to peak cross sections from the tensor force, and these cross sections require smaller reductions to match the data. However, the differential sensitivity for different states to changes in the individual components of the force, as illustrated above for the two versions of the M3Y force, suggests caution in attempting

to make empirical adjustments to the interaction to obtain a fit to the limited set of data presented in this paper.

VI. SUMMARY AND DISCUSSION

The $^{12}\text{C}(n,p)^{12}\text{B}$ reaction has been studied at 60 and 65 MeV and compared to earlier 56.3-MeV data. The experimental cross sections agree well when plotted as a function of momentum transfer. The (n,p) data also agree well with measured (p,p') and (p,n) data at about the same energies. Microscopic DWBA calculations, using one-body density-matrix elements from $0\hbar\omega$ and $1\hbar\omega$ shell-model calculations and the M3Y G matrix, have been carried out for states contributing to the peaks at 0 MeV (1^+ and 2^+), 4.4 MeV (2^- and 4^-), and 7.7 MeV (mainly 1^-). Calculations for pure LS OBDME's represent an attempt to make clear the origin of the important contributions to the cross sections at our incident energies, for which $|J_{\sigma\tau}|$ and $|J_{\tau}|$ are comparable in value. The angular distributions for all three peaks (strictly the $6 \rightarrow 9.5$ MeV region rather than a 7.7-MeV peak) are well reproduced when the shell-model OBDME's for the most important contributing states are used in the DWBA calculations. The calculated cross sections are, however, too large. In part, this is because the M3Y G -matrix interaction overestimates cross sections by, e.g., a factor of 1.6 for the 1^+ state. In contrast, for the 100–200-MeV range of incident energy, t -matrix interactions do well in accounting for the 1^+ cross section once the nuclear structure input is normalized to β decay.

Gaarde *et al.*¹⁴ have made a detailed study of spin-dipole strength in the $^{12}\text{C}(p,n)^{12}\text{N}$ reaction using a structure model which is quantitatively very similar to our full $1\hbar\omega$ model for moderate excitation energies. They find, with the use of HO single-particle wave functions in their DWBA calculations, that the calculated strength exceeds that observed in the energy region up to 12 MeV by roughly a factor of 2. They then suggest that the spin-dipole strength may be pushed further up in energy than the $1\hbar\omega$ shell model predicts. We have considered two effects which can account for much of the discrepancy referred to above without changing the distribution of dipole or spin-dipole strength, for which we would expect the shell model to be reliable.

The first effect is the use of WS wave functions, which reduces the cross sections by about 30%. We have argued that this is a genuine effect for the loosely bound $1s$ and $0d$ orbitals, in agreement with a similar investigation by Ohnuma *et al.*,⁵³ and that the commonly used well-depth prescription gives a reasonable approximation for the single-particle wave functions. The magnitude of the effect clearly depends on many details, including absorption, which varies with incident energy. Nevertheless, comparable effects occur in plane-wave Born approximation (PWBA) calculations for electron scattering. For the positive-parity excited states, realistic single-particle radial overlap functions are more difficult to calculate given that the effects of the Pauli principle and the bound-state effective interaction usually result in a strong fragmenta-

tion of single-nucleon pickup strength within a major shell.

The second effect that we include is an estimate of the effect of ground-state correlations. This is often demonstrated through the use of the schematic model.^{81,82} The Tamm-Dancoff approximation (TDA), which corresponds to calculations with a $0\hbar\omega$ ground state and $1\hbar\omega$ excited states, as in this paper and in Ref. 14, conserves the sum-rule strength, as embodied in Eq. (1), for p-h excitations. The random-phase approximation, on the other hand, conserves the energy-weighted sum rule, and the sum-rule strength, in the case of degenerate single-particle energies, goes as ϵ/E times the TDA sum-rule strength, with ϵ the unperturbed p-h energy and E the actual energy of the vibrational state. If, for arguments sake, we take $\epsilon=16$ MeV ($\sim 1\hbar\omega$) for ^{12}C and $E=22.7$ MeV for the dipole or spin-dipole resonance (the schematic-model arguments are valid in either case⁸³), we find a 30% reduction in the sum-rule strength due to RPA correlations. This is in reasonable agreement with Sagawa and Brown's perturbation estimate⁴³ of the effect of 2p-2h correlations in the ^{12}C ground state, which is probably an underestimate of the full effect of all correlations. Exactly the same effects apply to the effective one-body operators for first-forbidden β decay.

If we take the cross sections calculated using our structure model, the M3Y interaction, Woods-Saxon single-particle wave functions, and Sagawa and Brown's correction for ground-state correlations, we find that normalization factors of about 0.63, 0.71, and 0.61 are still required for the g.s. and 4.4- and 7.7-MeV peaks, respectively. This estimate assumes that the 1_3^- , 1_4^- , 2_3^- and 2_4^- model states contribute to the 7.7-MeV peak. If the 1_5^- and 0_2^- states, predicted just above 9 MeV in excitation energy, are also included, a normalization factor of 0.47 is needed. These normalization factors are typical of those required in previous studies which use the M3Y interaction. We conclude that, subject to considerable uncertainties in background subtractions, the treatment of unbound states, and other details, the cross sections for dipole and spin-dipole states up to 10 MeV or so in excitation energy in ^{12}B could be reproduced with an effective interaction for inelastic scattering that reproduces the low- q cross sections for well-understood p-shell states.

ACKNOWLEDGMENTS

We thank W. G. Love and J. Rapaport for many informative conversations and C. D. Goodman and J. Rapaport for comments on a draft of this paper. This work has been supported by the National Science Foundation under Grant No. PHY-8722008 and by the U.S. Department of Energy under Contract No. DE-AC02-76CH00016.

APPENDIX

In the direct term of the DWBA integral for inelastic nucleon scattering (Ref. 54, p. 658), the NN interaction enters as a function of $\mathbf{r}_i - \mathbf{r}_0$, where \mathbf{r}_0 and \mathbf{r}_i are the coordinates of the incident and struck nucleons referred

to an arbitrary origin. A Yukawa interaction, e.g., can then be expanded into functions of $\mathbf{r}_i - \mathbf{R}_A$ and $\mathbf{r}_0 - \mathbf{R}_A$, where \mathbf{R}_A is the center of mass coordinate for the nucleus. Then $\mathbf{r}_0 - \mathbf{R}_A$ is just the distorted-wave coordinate and the one-body transition density is required as a function of $\mathbf{r}_{iC} = [A/(A-1)](\mathbf{r}_i - \mathbf{R}_A)$, the relative coordinate between the struck nucleon and the $A-1$ core, rather than \mathbf{r}_i as in the conventional shell model. A coordinate transformation from $\mathbf{R}_{A-1}, \mathbf{r}_i$ to $\mathbf{R}_A, \mathbf{r}_{iC}$, which is possible for harmonic-oscillator wave functions, must be made. After the transformation is made, WS wave functions, for which \mathbf{r}_{iC} is the appropriate coordinate, can be used as single-particle wave functions. The procedure is described in Sec. III B of Ref. 40. It involves the insertion of a complete set of shell-model eigenstates between the creation and annihilation operators in the OBDME's. Since the shell-model eigenstates represent physical states of the core, a separation energy and a specific contribution to total transition density can be associated with each core state.

With the restriction to $0\hbar\omega$ and $1\hbar\omega$ shell-model configurations made in this paper, the result of summing over all $0\hbar\omega$ core states for $p \rightarrow p$ or $p \rightarrow sd$ transitions is to yield relative OBDME's which are larger than the conventional shell-model OBDME's by a factor $[A/(A-1)]^{Q/2}$, where $Q=Q_1+Q_2$ is the number of quanta for the two orbits involved in the transition. The appropriate oscillator parameter is $b_r = [A/(A-1)]^{1/2}b_0$ and the HO wave functions are functions of r_{iC}/b_r .

The sum over $1\hbar\omega$ core states, which involves linear combinations of s^3p^n and $s^4p^{n-2}sd$ configurations, gives rise to $s \rightarrow s$ or $s \rightarrow p$ contributions to the transition density. The relevant OBDME's, summed over all core states, can be obtained by equating, for the two coordinate systems, the matrix elements the identity or $\mathbf{r} - \mathbf{R}_A$ in coordinate space combined with the identity, σ , τ , or $\sigma \cdot \tau$ in spin-isospin space.

For $s \rightarrow p$ OBDME's, which transform as (10) under SU(3) with $\Delta L=1$, the contributions to the matrix elements of \mathbf{r} are just

$$T_{sp} = C_0^{(10)}(s \rightarrow p) O_0^{(10)}(s \rightarrow p) \quad (\text{A1})$$

and

$$T_{pd} = C_0^{(10)}(p \rightarrow sd) O_0^{(10)}(p \rightarrow sd), \quad (\text{A2})$$

where the C_0 coefficients are basically the conventional single-particle matrix elements of \mathbf{r} (note that for non-spurious shell-model wave functions, the matrix elements of \mathbf{R}_A are zero), and $C_0(p \rightarrow sd) = 2C_0(s \rightarrow p)$. Since coordinate transformations are independent of ΔT and ΔS , the equation

$$T_{sp} + T_{pd} = \left[\frac{A}{A-1} \right]^{3/2} \left[\frac{A}{A-1} \right]^{1/2} \left[\frac{A-1}{A} \right] T_{pd} + O_r^{(10)} \left[\frac{A}{A-1} \right]^{1/2} \left[\frac{A-1}{A} \right] \quad (\text{A3})$$

holds for the relative $s \rightarrow p$ OBDME's in each case, yielding

$$O_r^{(10)} = \left[\frac{A}{A-1} \right]^{1/2} \left[T_{sp} - \frac{1}{A} T_{pd} \right]. \quad (\text{A4})$$

For $\Delta J=1$, the LS to jj transformation relates the $0s_{1/2} \rightarrow 0p_{1/2}$ and $0s_{1/2} \rightarrow 0p_{3/2}$ OBDME's to those for $\Delta S=0$ and 1. Alternatively, one can work in jj coupling and write a pair of equations similar to those above for the matrix elements of \mathbf{r} and $\mathbf{r} \times \boldsymbol{\sigma}$.

The $0s \rightarrow 0s$ OBDME's for $\Delta J=0$ vanish unless the initial and final states are identical. Then, for $\Delta T=0$,

$$O_r^{(00)}(s \rightarrow s) = \frac{3}{2} \frac{A}{A-1}, \quad (\text{A5})$$

and for $\Delta T=1$,

$$O_r^{(00)}(s \rightarrow s) = -\frac{1}{A-1} \sqrt{T(T+1)}, \quad (\text{A6})$$

from which one can check that the number of $0s$ neutrons and protons are $2-(N-2)/(A-1)$ and $2-(Z-2)/$

$(A-1)$, respectively. For $\Delta J=1$ ($\Delta S=1$),

$$O_r^{(00)}(s \rightarrow s) = -\frac{1}{A-1} \sqrt{3} O_0^{(00)}(p \rightarrow p), \quad (\text{A7})$$

independent of ΔT . As stated above, the relative OBDME's can also be obtained from the shell-model calculation by summing over intermediate states. Since the $0s$ hole states are deeply bound, there is little point in breaking the sum up into contributions from individual core states.

One could also argue that there is little point in undertaking the coordinate transformations described in this appendix when then the shell-model wave functions provide a relatively poor description of experimental data. However, one frequently sees attempts to deal with center-of-mass effects, for which there is a simple prescription when HO wave functions are used in calculations of (e, e') form factors, by the introduction of $A/(A-1)$ scaling factors. Strictly, this is incorrect since the polynomials in the polynomial-times-Gaussian coordinate-space transition densities are generally changed in form by coordinate transformations.

*Present address: Rockwell International, Canoga Park, CA 91304.

†Present address: P-15, Los Alamos National Laboratory, Los Alamos, NM 87545.

¹G. Needham, F. P. Brady, D. H. Fitzgerald, J. L. Romero, J. L. Ullmann, J. W. Watson, C. Zanelli, N. S. P. King, and G. R. Satchler, Nucl. Phys. **A385**, 349 (1982).

²F. P. Brady and G. A. Needham, in *The (p, n) Reaction and Nucleon-Nucleon Force*, edited by C. D. Goodman, S. M. Austin, S. D. Bloom, J. Rapaport, and G. R. Satchler (Plenum, New York, 1980), p. 357.

³F. P. Brady, G. A. Needham, J. L. Ullmann, C. M. Castaneda, T. D. Ford, N. S. P. King, J. L. Romero, M. L. Webb, V. R. Brown, and C. H. Poppe, J. Phys. G **10**, 363 (1984).

⁴F. P. Brady, Can. J. Phys. **65**, 578 (1987).

⁵F. Ajzenberg-Selove, Nucl. Phys. **A506**, 1 (1990).

⁶W. C. Barber, Annu. Rev. Nucl. Sci. **12**, 1 (1962).

⁷D. Kurath, Phys. Rev. **130**, 1525 (1963).

⁸N. Vinh-Mau and G. E. Brown, Nucl. Phys. **29**, 89 (1962).

⁹S. Cohen and D. Kurath, Nucl. Phys. **73**, 1 (1965).

¹⁰F. H. Lewis and J. D. Walecka, Phys. Rev. **133**, B849 (1964); T. W. Donnelly, J. D. Walecka, I. Sick, and E. B. Hughes, Phys. Rev. Lett. **21**, 1196 (1968); T. W. Donnelly, Phys. Rev. C **1**, 833 (1970).

¹¹P. Antony-Spies, Nucl. Phys. **A188**, 641 (1972).

¹²R. S. Hicks, J. B. Flanz, R. A. Lindgren, G. A. Peterson, L. W. Fagg, and D. J. Millener, Phys. Rev. C **30**, 1 (1984).

¹³A. Yamaguchi, T. Terasawa, K. Nakahara, and Y. Torizuka, Phys. Rev. C **3**, 1750 (1971).

¹⁴C. Gaarde, J. S. Larsen, H. Sagawa, N. Ohtsuka, J. Rapaport, T. N. Taddeucci, C. D. Goodman, C. C. Foster, C. A. Goulding, D. Horen, T. Masterson, and E. Sugarbaker, Nucl. Phys. **A422**, 189 (1984).

¹⁵D. P. Stahel, R. Jahn, G. J. Wozniak, and J. Cerny, Phys. Rev. C **20**, 1680 (1979).

¹⁶K. G. Beard, J. Kasagi, E. Kashy, B. H. Wildenthal, D. L.

Freisal, H. Nann, and R. E. Warner, Phys. Rev. C **26**, 720 (1982).

¹⁷T. Motobayashi, H. Sakai, N. Matsuoka, T. Saito, K. Hosono, A. Okihana, M. Ishihara, S. Shimoura, and A. Sakaguchi, Phys. Rev. C **34**, 2365 (1986).

¹⁸J. A. Bistirlich, K. M. Crowe, A. S. L. Parsons, P. Sharek, and P. Truöl, Phys. Rev. C **5**, 1867 (1972).

¹⁹H. W. Baer, K. M. Crowe, and P. Truöl, Adv. Nucl. Phys. **9**, 177 (1977).

²⁰J. P. Perroud, A. Perrenoud, J. C. Alder, B. Gabioud, C. Joseph, J. F. Loude, N. Morel, M. T. Tran, E. Winkelmann, H. von Fellenberg, G. Strassner, P. Truöl, W. Dahme, H. Panke, and D. Renker, Nucl. Phys. **A453**, 542 (1986), and references therein.

²¹K. C. So, K. Min, L. Y. Murphy, E. J. Winhold, M. Yamazaki, P. Yergin, R. W. Gothe, B. Schoch, C. Bennhold, L. Tiator, S. J. Hall, J. D. Kellie, I. J. D. MacGregor, R. O. Owens, and D. Branford, Nucl. Phys. **A517**, 473 (1990).

²²J. Rapaport, T. Taddeucci, C. Gaarde, C. D. Goodman, C. C. Foster, C. A. Goulding, D. Horen, E. Sugarbaker, T. G. Masterson, and D. Lind, Phys. Rev. C **24**, 335 (1981).

²³C. A. Goulding, M. B. Greenfield, C. C. Foster, T. E. Ward, J. Rapaport, D. E. Bainum, and C. D. Goodman, Nucl. Phys. **A331**, 29 (1979).

²⁴B. D. Anderson, J. N. Knudson, R. Madey, and C. C. Foster, Nucl. Instrum. Methods **169**, 153 (1980).

²⁵W. A. Sterrenburg, M. N. Harakeh, S. Y. van der Werf, and A. van der Woude, Nucl. Phys. **A405**, 109 (1983).

²⁶I. Bergqvist, A. Brockstedt, L. Carlén, L. P. Ekström, B. Jakobsson, C. Ellegaard, C. Gaarde, J. S. Larsen, C. Goodman, M. Bedjidian, D. Contardo, J. Y. Grossiord, A. Guichard, R. Haroutunian, J. R. Pizzi, D. Bachelier, J. L. Boyard, T. Hennino, J. C. Jourdain, M. Roy-Stephan, M. Boivin, and P. Radvanyi, Nucl. Phys. **A469**, 648 (1987).

²⁷H. Okamura, A. Sakaguchi, S. Hatori, H. Sakai, N. Matsuoka, M. Fujiwara, T. Noro, T. Motobayashi, S. Satoh, A. Okihana,

- T. Yamaya, O. Satoh, and S.-I. Hayakawa, *Phys. Lett. B* **227**, 204 (1989).
- ²⁸K. P. Jackson, A. Celler, W. P. Alford, K. Raywood, R. Abegg, R. E. Azuma, C. K. Campbell, S. El-Kateb, D. Frekers, P. W. Green, O. Häusser, R. L. Helmer, R. S. Henderson, K. H. Hicks, R. Jeppesen, P. Lewis, C. A. Miller, A. Moalem, M. A. Moinester, R. B. Schubank, G. G. Shute, B. M. Spicer, M. C. Vetterli, A. I. Yavin, and S. Yen, *Phys. Lett. B* **201**, 25 (1988).
- ²⁹J. A. Jungerman and F. P. Brady, *Nucl. Instrum. Methods* **89**, 167 (1970).
- ³⁰G. Needham, Ph.D. thesis, University of California, Davis, 1980.
- ³¹T. D. Ford, Ph.D. thesis, University of California, Davis, 1985.
- ³²T. D. Ford, G. A. Needham, F. P. Brady, J. L. Romero, and C. M. Castaneda, *Nucl. Instrum. Methods* **228**, 81 (1984).
- ³³T. D. Ford, F. P. Brady, C. M. Castaneda, J. R. Drummond, B. McEachern, J. L. Romero, and D. S. Sorenson, *Nucl. Instrum. Methods* **A274**, 253 (1988).
- ³⁴N. S. P. King, J. D. Reber, J. L. Romero, D. H. Fitzgerald, J. L. Ullmann, T. S. Subramanian, and F. P. Brady, *Phys. Rev. C* **21**, 1185 (1980).
- ³⁵R. Schaeffer and J. Raynal, Program DWBA70 (unpublished); extended version DW81 by J. R. Comfort (unpublished).
- ³⁶J. R. Comfort and B. C. Karp, *Phys. Rev. C* **21**, 2162 (1979).
- ³⁷G. Bertsch, J. Boryzovicz, H. McManus, and W. G. Love, *Nucl. Phys. A* **284**, 399 (1977).
- ³⁸W. G. Love (Ref. 3), p. 23.
- ³⁹S. Cohen and D. Kurath, *Nucl. Phys.* **73**, 1 (1965).
- ⁴⁰D. J. Millener, J. W. Olness, E. K. Warburton, and S. S. Hanna, *Phys. Rev. C* **28**, 497 (1983).
- ⁴¹D. J. Millener and D. Kurath, *Nucl. Phys. A* **255**, 315 (1975).
- ⁴²D. M. Brink and G. R. Satchler, *Angular Momentum* (Clarendon, Oxford, 1968).
- ⁴³H. Sagawa and B. A. Brown, *Phys. Lett.* **143B**, 283 (1984).
- ⁴⁴B. Castel and A. G. M. van Hees, *Phys. Rev. C* **28**, 2571 (1983).
- ⁴⁵B. Castel, I. P. Johnstone, and A. G. M. van Hees, *Phys. Rev. C* **32**, 323 (1985).
- ⁴⁶D. J. Millener, D. E. Alburger, E. K. Warburton, and D. H. Wilkinson, *Phys. Rev. C* **26**, 1167 (1982).
- ⁴⁷J. R. Comfort, G. L. Moake, C. C. Foster, P. Schwandt, and W. G. Love, *Phys. Rev. C* **26**, 1800 (1982), and references therein.
- ⁴⁸S. Cohen and D. Kurath, *Nucl. Phys. A* **101**, 1 (1967).
- ⁴⁹J. Dubach and W. C. Haxton, *Phys. Rev. Lett.* **41**, 1453 (1978).
- ⁵⁰D. J. Millener, in *Pion-Nucleus Physics: Future Directions and New Facilities at LAMPF*, edited by R. J. Peterson and D. D. Strottman, AIP Conf. Proc. 163 (AIP, New York, 1988), p. 402.
- ⁵¹D. J. Millener, D. I. Sober, H. Crannell, J. T. O'Brien, L. W. Fagg, S. Kowalski, C. F. Williamson, and L. Lapiakás, *Phys. Rev. C* **39**, 14 (1989).
- ⁵²B. L. Clausen, R. J. Peterson, and R. A. Lindgren, *Phys. Rev. C* **38**, 589 (1988).
- ⁵³H. Ohnuma, M. Kabasawa, K. Furukawa, T. Kawamura, Y. Takahashi, A. Satoh, T. Nagagawa, K. Maeda, K. Miura, T. Niizeki, and H. Orihara, *Nucl. Phys. A* **467**, 61 (1987).
- ⁵⁴G. R. Satchler, *Direct Nuclear Reactions* (Oxford University Press, New York, 1983), pp. 803–805.
- ⁵⁵U. Deutschmann, G. Lahm, R. Neuhausen, and J. C. Bergstrom, *Nucl. Phys. A* **411**, 337 (1983).
- ⁵⁶B. T. Chertok, C. Sheffield, J. W. Lightbody, Jr., S. Penner, and D. Blum, *Phys. Rev. C* **8**, 23 (1973).
- ⁵⁷R. S. Hicks, R. L. Huffman, R. A. Lindgren, G. A. Peterson, M. A. Plum, and J. Button-Shafer, *Phys. Rev. C* **36**, 485 (1987).
- ⁵⁸B. A. Brown and B. H. Wildenthal, *Nucl. Phys. A* **474**, 290 (1987).
- ⁵⁹I. S. Towner and F. C. Khanna, *Nucl. Phys. A* **399**, 334 (1983).
- ⁶⁰A. Arima, K. Shimizu, W. Bentz, and H. Hyuga, *Adv. Nucl. Phys.* **18**, 1 (1987).
- ⁶¹T. Suzuki, H. Hyuga, A. Arima, and K. Yazaki, *Phys. Lett.* **106B**, 19 (1981).
- ⁶²A. Friebel, P. Manakos, A. Richter, E. Spamer, W. Stock, and O. Titze, *Nucl. Phys. A* **294**, 129 (1978).
- ⁶³L. Tiator, C. Bennhold, and R. Neuhausen, *Nucl. Phys. A* **501**, 751 (1989).
- ⁶⁴K. Hosono, M. Kondo, T. Saito, N. Matsuoka, S. Nagamachi, S. Kato, K. Ogino, Y. Kadota, and T. Noro, *Phys. Rev. Lett.* **41**, 621 (1978).
- ⁶⁵R. O. Lane, C. E. Nelson, J. L. Adams, J. E. Monahan, A. J. Elwyn, F. P. Mooring, and A. Langsdorf, Jr., *Phys. Rev. C* **2**, 2097 (1970).
- ⁶⁶K. Min, E. J. Winhold, K. Shoda, H. Tsubota, H. Ohashi, and M. Yamazaki, *Phys. Rev. Lett.* **44**, 1384 (1980).
- ⁶⁷K. W. Jones, C. Glashauser, S. Nanda, R. de Swiniarski, T. A. Carey, W. Cornelius, J. M. Moss, J. B. McClelland, S. J. Seestrom-Morris, J. R. Comfort, J.-L. Escudie, M. Gazzaly, N. Hintz, G. Igo, M. Haji-Saeid, and C. A. Whitten, *Phys. Lett.* **128B**, 281 (1983).
- ⁶⁸W. G. Love, A. Klein, M. A. Franey, and K. Nakayama, *Can. J. Phys.* **65**, 536 (1987).
- ⁶⁹M. A. Franey and W. G. Love, *Phys. Rev. C* **31**, 488 (1985).
- ⁷⁰F. Petrovich, W. G. Love, and R. J. McCarthy, *Phys. Rev. C* **21**, 1718 (1980).
- ⁷¹T. N. Taddeucci, C. A. Goulding, T. A. Carey, R. C. Byrd, C. D. Goodman, C. Gaarde, J. Larsen, D. Horen, J. Rapaport, and E. Sugarbaker, *Nucl. Phys. A* **469**, 125 (1987).
- ⁷²J. Rapaport, in *Fundamental Symmetries and Nuclear Structure*, edited by J. N. Ginocchio and S. P. Rosen (World Scientific, Singapore, 1989), p. 186.
- ⁷³F. Petrovich (Ref. 3), p. 115.
- ⁷⁴F. Petrovich, R. H. Howell, C. H. Poppe, S. M. Austin, and G. M. Crawley, *Nucl. Phys. A* **383**, 355 (1982).
- ⁷⁵W. G. Love and M. A. Franey, *Phys. Rev. C* **24**, 1073 (1981); **27**, 438(E) (1983).
- ⁷⁶D. S. Sorenson, Ph.D. thesis, University of California, Davis, 1990.
- ⁷⁷W. G. Love (private communication).
- ⁷⁸H. Ohnuma and H. Orihara, *Prog. Theor. Phys.* **67**, 353 (1982).
- ⁷⁹M. Yabe, A. Hosaka, K.-I. Kubo, and H. Toki, *Prog. Theor. Phys.* **73**, 1165 (1985).
- ⁸⁰A. Hosaka, K.-I. Kubo, and H. Toki, *Nucl. Phys. A* **444**, 76 (1985).
- ⁸¹G. E. Brown, *Unified Theory of Nuclear Models and Forces* (North-Holland, Amsterdam, 1967).
- ⁸²I. S. Towner, *A Shell Model Description of Light Nuclei* (Oxford University Press, New York, 1977).
- ⁸³I. S. Towner, B. Castel, and L. Zamick, *Nucl. Phys. A* **365**, 189 (1981).